A STUDY OF CONFORMATIONAL FEATURES OF DISTAMYCIN-DNA AND NETROPSIN-DNA COMPLEXES BY RAMAN SPECTROSCOPY

A THESIS

Presented to

The Faculty of the Division of Graduate

Studies and Research

by

James Carey Martin

In Partial Fulfillment

of the Requirements for the Degree

Doctor of Philosophy

in the School of Physics

Georgia Institute of Technology

August, 1978

A STUDY OF CONFORMATIONAL FEATURES OF DISTAMYCIN-DNA AND NETROPSIN-DNA COMPLEXES BY RAMAN SPECTROSCOPY

Approved:

D. C. O'Shea, Chairman

Roger M. Wartell

Nai-Tang Yu

Date approved by Chairman 8/1/78

TO KATHLEEN

SUMMARY

The binding of distamycin A and netropsin to duplex DNA has been studied by Raman spectroscopy. Several changes occur in the Raman spectra of these drugs upon binding DNA. These changes were analyzed by assigning specific motions to the observed Raman bands through the use of molecular subunits of the drugs and normal mode calculations. Analysis indicates that pyrrole ring and peptide group vibrations are altered upon binding to DNA. The environment of the pyrrole ring methyl groups are not affected by the binding. This data provides physical evidence consistent with a binding model in which the methyl groups on the pyrroles project away from the DNA and the peptide N-H groups form hydrogen bonds with the DNA.

ACKNOWLEDGMENTS

The author wishes to express sincere appreciation to Dr. D.C. O'Shea for his support as thesis advisor. His insight in the experimental portion of this work has been particularly valuable.

I would like to thank my reading committee for their interest and advice. Special gratitude is due to Dr. Roger Wartell, whose scientific wisdom, untiring assistance and inspiration have made possible the completion of this work.

During my graduate studies I have particularly appreciated the friendship of Dr. John Shelnutt, around whom life is always interesting.

Most of all I would like to thank Kathleen. The love, understanding, support and sacrifice of my wife have made graduate study possible for me.

TABLE OF CONTENTS

Page

ACKNOWLEDGMENTS iii

LIST OF TABLES v

LIST OF ILLUSTRATIONS vi

Chapter

I. INTRODUCTION 1

DNA-protein Interactions
Antiobiotics Netropsin and Distamycin A and Their Binding to DNA
Introduction to Raman Scattering
Classical Description of Raman Scattering
Quantum Mechanical Outline of Raman Scattering

II. EXPERIMENTAL EQUIPMENT, MATERIALS AND METHODS . . 24

Raman Instrumentation
Sample Materials
Analysis Methods

III. NORMAL COORDINATE CALCULATIONS 37

Basic Theory
Computational Approaches
Force Fields

IV. RESULTS AND DISCUSSION 58

Normal Coordinate Calculations
Raman Spectra of Netropsin and Distamycin A
Drug-DNA Complexes

V. CONCLUSIONS 71

Summary of Binding Results
Geometric Feature of the Binding Model

APPENDICES 75

BIBLIOGRAPHY 85

VITA 88

LIST OF TABLES

Table		Page
1	Abbreviations Frequently Used in this Research	2
2	Raman Group Frequencies	35
3	Frequency Correlations Between Pyrrole and Two Derivatives.	60
4	Observed and Calculated Frequencies and Assignments for Distamycin	62

LIST OF ILLUSTRATIONS

Figure		Page
1	Chemical Structures of DNA and RNA	4
2	Bases Occurring in DNA and RNA	5
3	Chemical Structures of Netropsin, Distamycin A and a Model Fragment	8
4	Shapes of Netropsin and Distamycin A	9
5	Symmetric and Antisymmetric Stretching Vibrations	15
6	Raman System Diagram	25
7	Ultraviolet Absorption Spectra of Netropsin and Distamycin A	29
8	Subtraction of the 1645 cm^{-1} Water Band	33
9	Schematic Diagram of the Matrix Diagonalization Problem .	46
10	Characterization of Bond Changes as Bends and Stretches .	53
11	Distamycin A and Netropsin Spectra (950 cm^{-1})	65
12	Distamycin A Low Frequency Spectrum	66
13	Raman Spectra of Bound and Unbound Distamycin A	68

CHAPTER I

INTRODUCTION

The antibiotics netropsin and distamycin A, considered in this investigation, are of interest because of their ability to recognize and bind preferentially to duplex DNA regions of high adenine·thymine (A·T) composition.[1] (See Table 1 for abbreviations). This binding makes these drugs potentially useful in two different ways.

The first of these involves their antibiotic activity. Both netropsin and distamycin inhibit the replication of Shope fibroma and vaccinia viruses in mammalian cells[2,3]. Netropsin inhibits the growth of bacteria, mycobacteria and yeast[4]. In addition, distamycin inhibits experimental tumors in rats and mice, and exhibits a high antiviral activity for herpes simplex, zoster and adeno viruses[5-10]. Synthetic distamycin analogs show an enhanced antiviral activity and diminished cytotoxicity relative to distamycin[1,11]. Distamycin has been used clinically for the treatment of virus infections of the skin. Toxicity has prevented a wider application of netropsin and distamycin[12]. Information about their mode of binding might suggest chemical modifications leading to diminished toxicity.

Because of their specificity for A·T regions of duplex DNA, the drugs netropsin and distamycin are of interest in another context. They can be viewed as simplified models of proteins which bind to specific base pair sequences of DNA and regulate genetic processes. Because

Table 1. Abbreviation Frequently Used in This Research

A	adenine
C	cytosine
cm^{-1}	wavenumber or reciprocal centimeter
CRT	cathode ray tube
DNA	deoxyribonucleic acid
G	guanine
I	inosine
M	molar
mRNA	messenger ribonucleic acid
NCA	normal coordinate analysis
nm	nanometers
RNA	ribonucleic acid
T	thymine
UV	ultraviolet
CPK	Corey-Pauling-Kolthun

of the basic importance of site specific protein-DNA interactions in molecular biophysics, a brief review of this area is given below.

DNA-Protein Interactions

Deoxyribonucleic acid (DNA) is a two stranded polymer (see Figure 1) which has been shown to function as a repository of genetic information in organisms[13]. The genetic information is encoded by the specific sequence of four types of nucleotide subunits making up the DNA polymer. Each nucleotide subunit has three molecular groups: a cyclic deoxyribose sugar, a phosphate group, and a base. The bases are derivatives of purine and pyrimidine, which are aromatic heterocyclic compounds. The predominant bases in DNA adenine, guanine, cytosine, and thymine are shown in Figure 2. Each of the two strands of DNA consists of a polymeric backbone of deoxyribose sugars linked by phosphodiester bridges and the linear sequence of bases. The two strands wind around each other in a right handed helix and are held together by hydrogen bonds between adenine and thymine on opposite strands (A·T base pairs) and guanine and cytosine on opposite strands (G·C base pairs).

Utilization of DNA information requires a different class of macromolecules which bind reversibly to DNA. These molecules, the proteins, have the capability of creating specialized chemical environments. Proteins can be "designed" to have very specific conformations with complicated topologies. Regions of these macromolecules may be charged or neutral, hydrophilic or hydrophobic.

Proteins which bind to DNA have a range of different functions

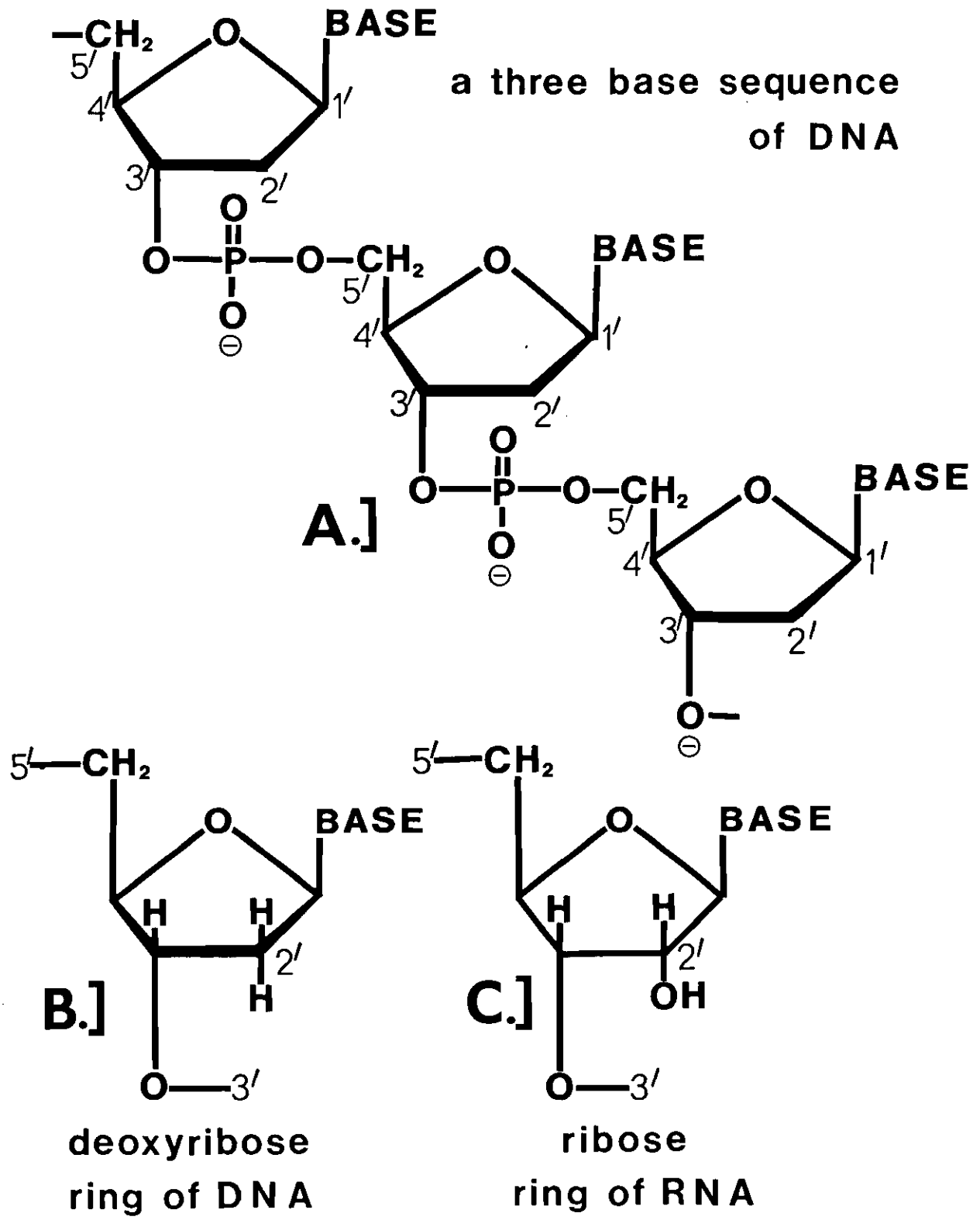

Figure 1. Chemical Structures of DNA and RNA.

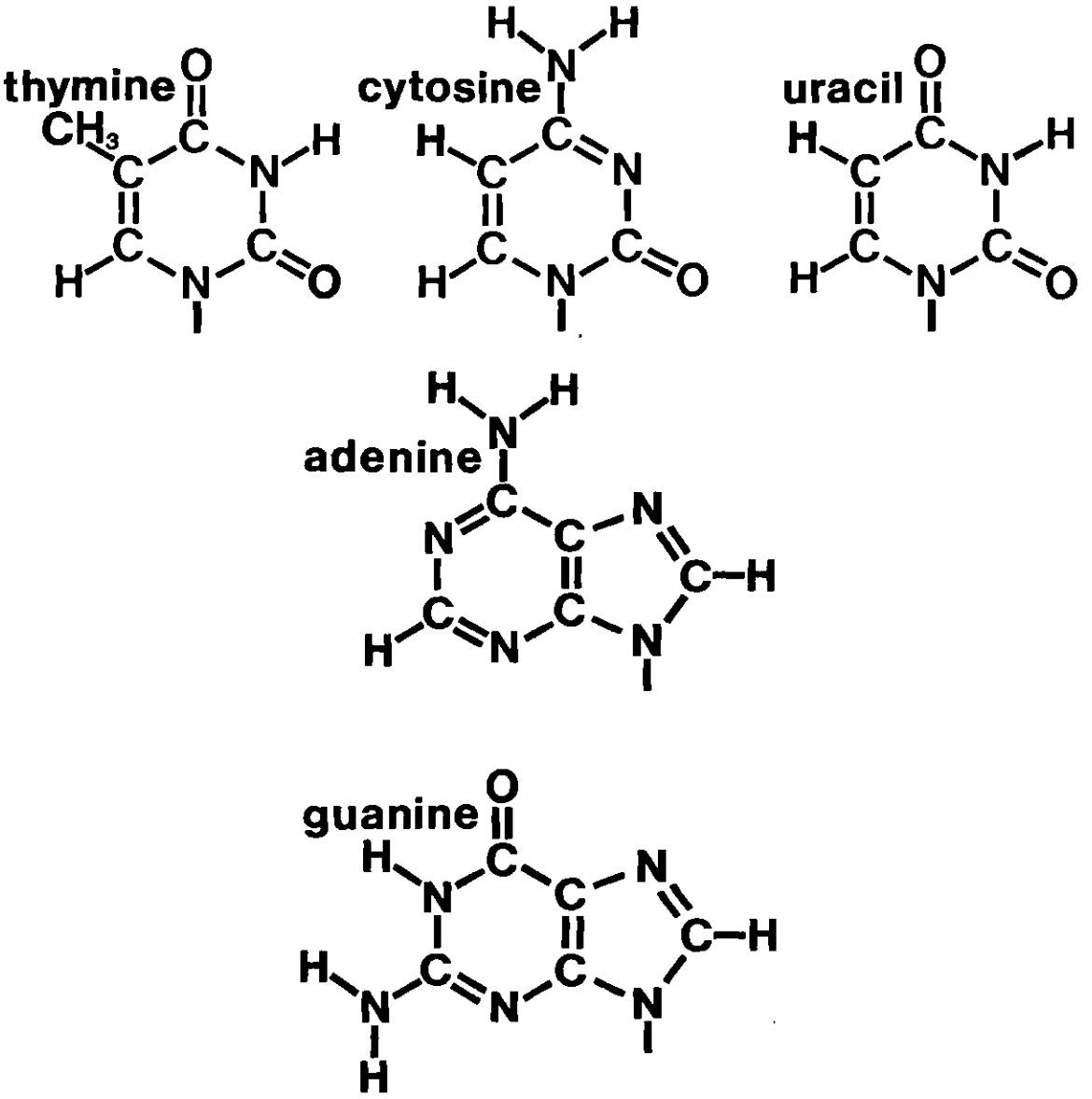

Figure 2. Bases Occurring in DNA and RNA.

including: 1) Associating non-specifically with DNA as a packaging medium, 2) Catalyzing various reactions in which DNA is replicated, repaired, transcribed into ribonucleic acid (RNA) form, and otherwise modified, 3) Regulating the transcription of specific portions of DNA. In the remainder of this discussion attention will be focused on the control of transcription.

Transcription is the first step of protein synthesis in a cell in which the strands of DNA are enzymatically "copied" into complementary RNA strands. The catalysis is performed by a class of proteins called RNA polymerase. Further steps in protein synthesis utilize this messenger RNA (mRNA) rather than the original DNA. Control of the synthesis of mRNA has been found to involve the highly selective binding of regulatory proteins to specific regions of DNA. This binding may interfere with the access of RNA polymerase to these DNA regions and thereby block transcription of DNA to mRNA.

The extreme specificity which regulatory proteins show for localized regions of DNA is the key to their activity. Regulatory proteins may bind to these special regions with up to one million times the affinity which they show for the other available DNA regions[14]. In spite of an extensive number of investigations a complete understanding of the interactions generating this binding is not available.

The specificity of regulatory protein-DNA binding suggests the necessity for several simultaneous favorable interactions. These interactions may include hydrogen bonding, electrostatic attraction, and hydrophobic effects. In order to study these modes of interaction simpler model systems, such as, polyamines, polypeptides, antibiotics,

and dyes have been employed[15]. The drugs used in the present investigation have simpler specificities and much smaller sizes than regulatory proteins. Studying these smaller molecules allows the possibility of a detailed description, not generally available for the larger proteins.

The Antibiotics Netropsin and Distamycin A and Their Binding to DNA

The chemical structures of netropsin and distamycin A are shown in Figure 3[16-20]. These drugs are related oligopeptides, each consisting of a central chromophoric region with side chains attached at opposite ends. The chromophores contain repeating N-methylpyrrole-2-carboxamide units. Netropsin has two such units and distamycin A has three. (Other distamycins may be synthesized with one to five repeating units). Both drugs have a positively charged amidinopropyl side chain. In netropsin the opposite side chain ends in a positively charged guanidinoacetyl group.

Distamycin has a formyl group with no net charge on the opposite end. In terms of overall structure these differences between the two drugs tend to offset each other to make the general shape and size of the drugs very similar (see Figure 4).

Previous investigations have yielded information about the binding of these drugs to DNA[1,21-25]. Sedimentation velocity studies show that these drugs do not unwind DNA[22,26]. This indicates that the drugs do not intercalate upon binding. The viscosity behavior of drug-DNA complexes indicates that netropsin elongates DNA, whereas distamycin may bend the DNA helix[21,27]. Several results indicate that both drugs bind in the minor groove of DNA: 1) Both drugs bind tightly to the DNA polymers poly d(I)·poly d(C) and poly d(I-C)·poly d(I-C) in 0.1M

a.]

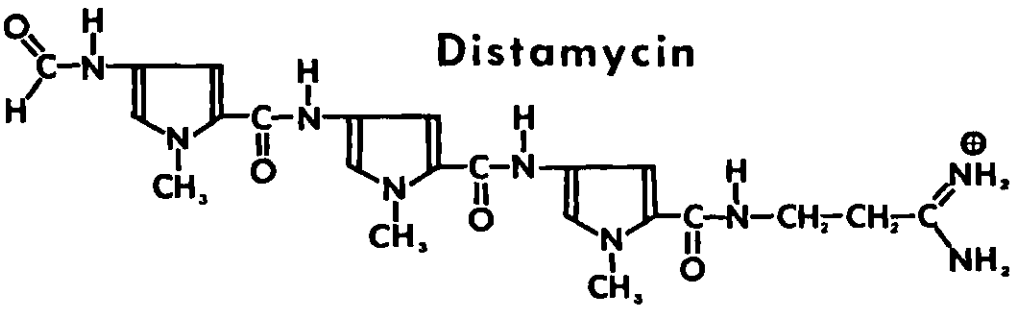

b.]

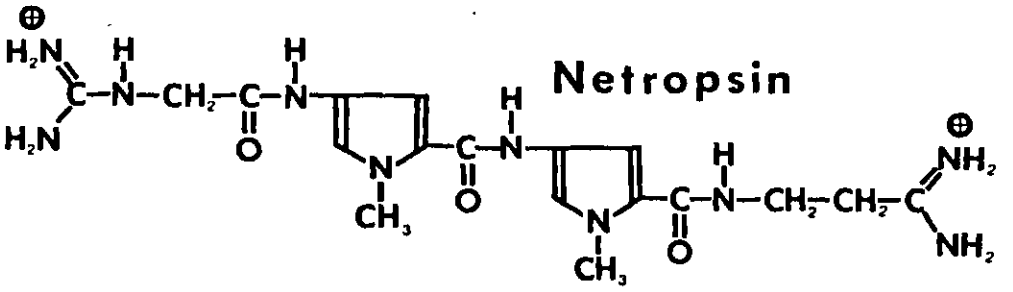

c.]

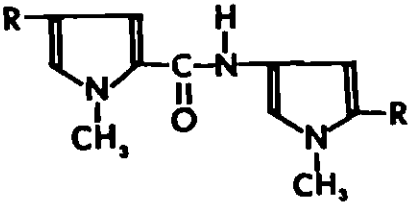

Figure 3. Chemical Structures of Netropsin, Distamycin A and a Model Fragment.

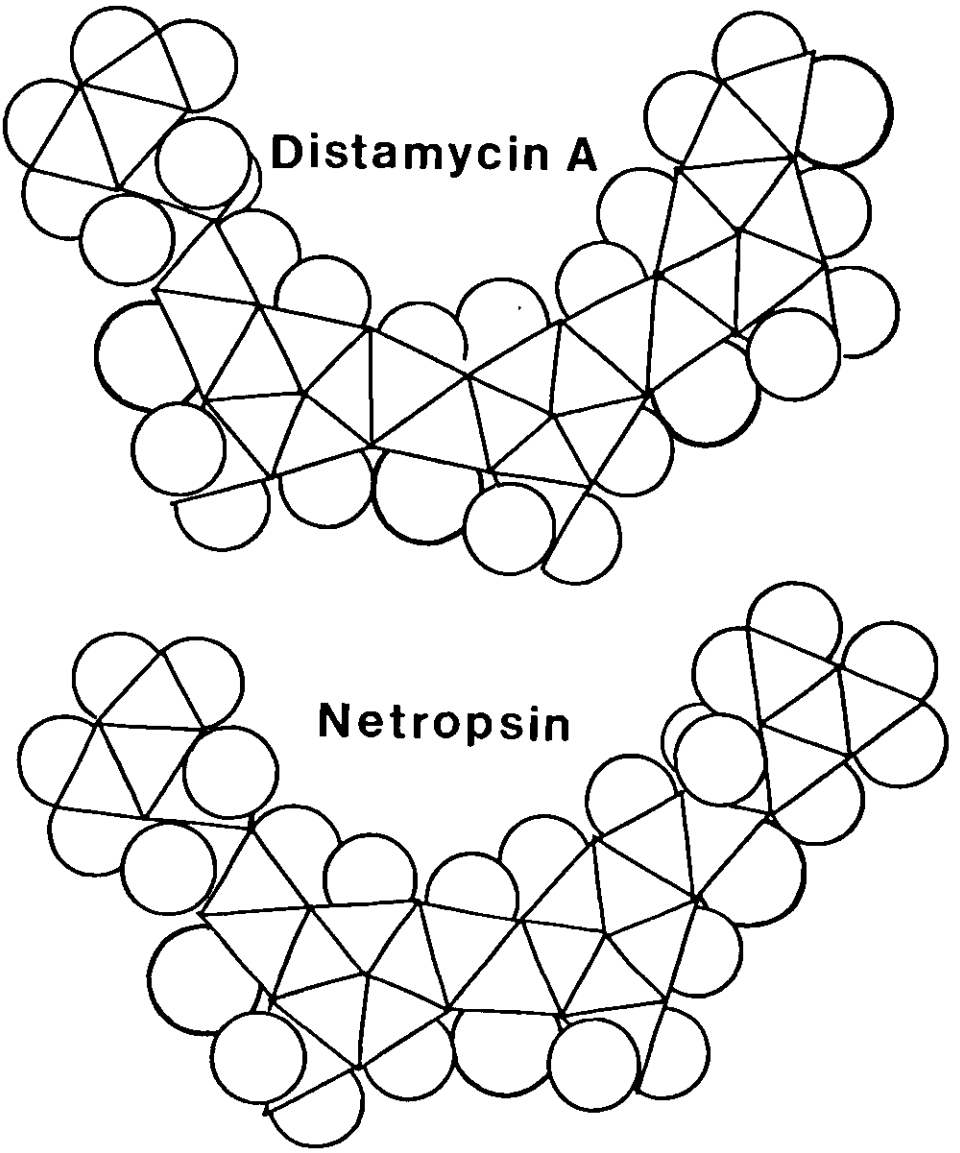

Figure 4. Shapes of Netropsin and Distamycin A.

sodium ion solutions, but show little or no binding to poly d(G)·poly d(C) and poly d(G-C) poly d(G-C)[1,22,23]. These pairs of DNAs differ only at the 2 position of the purine ring which always lies in the minor groove. 2) Adenine nitrogens in the minor groove of DNA are shielded from methylation by the binding of both drugs, while guanine nitrogens in the major groove remain unshielded[28]. Estimates of the number of base pairs covered per drug molecule range from 3 to 5 for netropsin. The value of 3 was obtained using a combination of UV spectral titrations and dialysis[22] and by means of analytical centrifugation[26]. The latter study suggests similar results for distamycin A. In contrast, the results of circular dichroism studies[24], have been interpreted to be consistent with the occupation of 5 base pairs by each netropsin molecule.

Introduction to Raman Scattering

The Raman effect is an inelastic scattering of light by the vibrational motions of the atoms of a material. This phenomenon was predicted theoretically in 1923 by Smekal[29] on the basis of simple quantum mechanical arguments. Five years later experimental evidence of the effect was given by C. V. Raman[30]. Due to the very small probability for this process, its spectroscopic usage was severely limited for some 40 years. With the advent of laser light sources and more sensitive methods of light detection, the applications of Raman spectroscopy have increased enormously. This technique is widely used in the analysis of molecular structures and interactions of biophysical interest[31,32].

While quantum mechanics must be used for a complete description of Raman scattering, classical considerations can show the main features

of this effect in a more intuitive way. Thus, the classical approach will be developed first, followed by a brief quantum mechanical description.

Classical Description of Raman Scattering

Classical electromagnetic theory predicts that a charged particle radiates when it is accelerated. This acceleration may be induced by the presence of the electromagnetic field due to incident light and may lead to "scattered" light. For extended systems of charges, such as molecules, the emitted power may be expressed in terms of the second time derivative of the electric dipole moment (see Appendix A). In a macroscopic sample the dipole moment per unit volume or polarization $\vec{P}$ is used. In Appendix A the expression for the average emitted power is shown to be:

$$\bar{p} = \frac{2V^2 \overline{\left(\frac{d^2P}{dt^2}\right)^2}}{3C^3} \qquad \text{(A-12)}$$

(Here V is the sample volume, C is the speed of light, and P is the polarization. The bar indicates time averaging of the quantity).

In order to characterize the scattered light, the time dependence of $\vec{P}$ must be investigated. For a sample in an intense light beam, the main time variation of $\vec{P}$ results from perturbations in the dipole moments of molecules caused by the oscillating electric field of the light. Thus, it is instructive to expand $\vec{P}$ in a Taylor series in terms of the applied electric field $\vec{E}$ due to the light. For a sample in a continuous wave laser beam with power of 1 watt focussed to a diameter of 600 $\mathring{A}$ the

electric field of the light $\vec{E}$ is less than 10^{-4} as large as the ambient interatomic electric field[33]. Thus under the usual experimental conditions for Raman scattering the electric field of the incident, light represents an extremely mild perturbation. For this reason the size of the terms in the Taylor series drops off extremely rapidly and only the first three terms need be considered. (With the use of pulsed lasers of peak power in the gigawatt range it is possible to generate much larger electric field changes. Under these conditions the previous approximation would have to be reevaluated.)

$$\vec{P}(\vec{E}) = \vec{P}(\vec{E}=0) + \sum_{i=1}^{3} \left.\frac{\partial \vec{P}}{\partial E_i}\right|_{\vec{E}=0} E_i + \frac{1}{2} \sum_{j=1}^{3} \sum_{k=1}^{3} \left.\frac{\partial^2 \vec{P}}{\partial E_j \partial E_k}\right|_{\vec{E}=0} E_j E_k \qquad \text{(I-1)}$$

$$+ \text{higher order terms}$$

The constant term in this expansion will be non-zero only for electrets, which have permanent net dipole moments per unit volume and will cause no time dependence. The second term in equation (I-1) gives the predominant contribution to $\vec{P}$ for most materials. In this equation the rate of change of $\vec{P}$ with the i-th component of the external electric field vector E_i is called the polarizability per unit volume $\vec{\alpha}_i$. Using this definition, Eq.(I-1) may be written as:

$$\vec{P}(\vec{E}) = \vec{P}(\vec{E}=0) + \sum_{i=1}^{3} \vec{\alpha}_i \Big|_{\vec{E}=0} E_i + \frac{1}{2} \sum_{j=1}^{3} \sum_{k=1}^{3} \left.\frac{\partial \vec{\alpha}_j}{\partial E_k}\right|_{\vec{E}=0} E_k E_j \qquad \text{(I-2)}$$

The second term describes a tensor relationship between $\vec{E}$ and $\vec{P}$. The elements of the polarizability tensor $\boldsymbol{\alpha}$ have the form

$$\alpha_{ij}\Big|_{\vec{E}=0} = \frac{\partial P_i}{\partial E_j}\Big|_{\vec{E}=0} \qquad \text{(I-3)}$$

Since these tensor elements are constants, the time dependence of this term is simply that of the applied electric field. The third term may be shown to have a more complicated variation with time which involves the molecular vibrations of the sample. In Appendix B the form of $\vec{P}(\vec{E})$ is worked out for a sample whose molecules are undergoing harmonic oscillation (with frequency ν) in the presence of a sinusoidally varying electric field (with frequency ν_ℓ). Under these conditions it is shown that the polarization becomes:

$$\vec{P}(\vec{E}) = \vec{P}_o + \vec{A}_o \cos 2\pi\, \nu_\ell t + B_o \{\cos 2\pi(\nu_\ell+\nu)t + \cos 2\pi(\nu_\ell-\nu)t\} \qquad \text{(A-23)}$$

where:

$$\vec{P}_o = \vec{P}(\vec{E} = 0)$$

$$\vec{A}_o = \boldsymbol{\alpha}_o \vec{E}_o \qquad \text{(A-22)}$$

$$\vec{B}_o = \frac{X_{o\nu}}{4}\boldsymbol{\beta}^{\nu}_o \vec{E}_o$$

and:

$X_{o\nu}$ = the amplitude of a vibrational parameter characterizing the normal vibration with frequency ν

$\boldsymbol{\beta}^{\nu}$ = the tensor whose elements β^{ν}_{ij} give the rate of change of the volume polarizability element α_{ij} with respect to the parameter $X\nu$. ($\boldsymbol{\beta}^{\nu}_o$ evaluated at $X\nu = 0$.).

$\vec{E}_o$ = the peak value of the electric field due to the indcident light

Since $\vec{P}_o$, $\vec{A}_o$, and $\vec{B}_o$ are time independent $\frac{d^2\vec{P}}{dt^2}$ may be calculated as:

$$\frac{d^2\vec{P}}{dt^2} = -(2\pi)^2 \{\vec{A}_o \nu_\ell^2 \cos 2\pi \nu_\ell t + \vec{B}_o(\nu_\ell+\nu)^2 \cos 2\pi(\nu_\ell+\nu)t + \vec{B}_o(\nu_\ell-\nu)^2 \cos 2\pi(\nu_\ell-\nu)t\} \quad \text{(I-4)}$$

When the expression for $\frac{d^2P}{dt^2}$ is squared, cross terms arise. However, since each of the terms in $\frac{d^2P}{dt^2}$ has a different time dependence, these cross terms average to zero. The final intensity thus involves only the three direct terms:

$$I \sim A_o^2 \nu_\ell^4 \cos^2 2\pi \nu_\ell t + B_o^2(\nu_\ell+\nu)^4 \cos^2 2\pi(\nu_\ell+\nu)t + B_o^2(\nu_\ell-\nu)^4 \cos^2 2\pi(\nu_\ell-\nu)t \quad \text{(I-5)}$$

The first term leads to Rayleigh scattering at the frequency of the incident light. The intensity of this component depends on the polarizability per unit volume of the sample. Since all materials are polarizable to one degree or another, Rayleigh scattering is observed generally. The following two terms predict Raman scattering at frequencies placed symmetrically about the frequency of the incident light. These latter two components depend for their intensity on the occurrence of a change in polarizability per unit volume during molecular vibrations (i.e. $\beta^\nu = \frac{\partial\alpha}{\partial X_\nu}$). Thus Raman scattering results when the ease with which a molecule is deformed by an external electric field varies during a certain vibrational motion. For example, consider the two vibrational modes of a linear triatomic molecule, shown in Figure 5. During motions of the symmetric stretching mode similar changes occur in the ability of

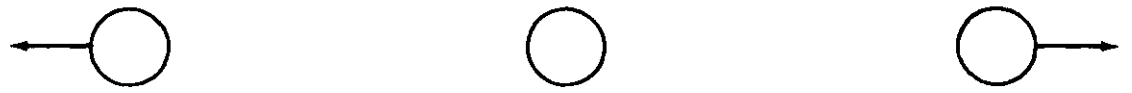

SYMMETRIC STRETCH

ANTI-SYMMETRIC STRETCH

Figure 5. Symmetric and Antisymmetric Stretching Vibrations.

both bonds to resist changes in polarization of the molecule. Thus, $\frac{\partial \alpha}{\partial X \nu}$ is relatively large in this case. In the antisymmetric stretching mode one bond becomes stiffer as the other becomes softer. The polarizability of the entire molecule thus stays relatively constant and $\frac{\partial \alpha}{\partial X \nu}$ is small.

The classical approach to Raman scattering predicts several observed features. These are: 1) the symmetric placement of Raman bands about the exciting frequency, 2) the fourth power dependence on frequency, 3) the weakness of Raman scattering as compared to Rayleigh scattering, 4) the relation of the intensity of Raman bands to polarizability changes during molecular vibrations. However, the classical approach incorrectly predicts that the intensity ratio of the higher frequency to lower frequency Raman components will be:

$$\frac{I_{\nu \ell + \nu}}{I_{\nu \ell - \nu}} = \frac{(\nu \ell + \nu)^4}{(\nu \ell - \nu)^4} > 1 \qquad \text{(I-6)}$$

(The lower frequency component is called the Stokes band in analogy to the Stokes fluoresence rule. The higher frequency component is called the anti-Stokes band.) Experimentally, this ratio is less than 1. An additional factor is necessary to resolve this discrepancy. This factor is due to quantum mechanical reasons and will be described below.

Quantum Mechanical Outline of Raman Scattering

When a quantum mechanical approach is used, several kinds of interactions are predicted between light and matter. These include absorption and emission of light as well as Rayleigh and Raman scattering. This approach[34,35] is quite lengthy and the details are not

essential to the present investigation. However, by providing a brief outline of this procedure, a clearer background may be provided concerning the source of Raman scattered light, its physical properties and relation to other light-matter interactions.

In order to describe the interaction of light with matter quantum mechanically, time dependent perturbation theory is used. Preliminary to this solutions must be described for a molecule and a radiation field which do not interact. The stationary energy states of an isolated molecule may be described by:

$$\hat{H}_{molecule}\ \psi_n(X) = E_n\ \psi_n(X) \tag{I-7}$$

$$\psi_n(X,t) = \psi_n(X)\ e^{-i\frac{E_n t}{\hbar}} \tag{I-8}$$

where $\psi_n(X)$ and $\psi_n(X,t)$ are the time independent and time dependent state functions of the molecule, $\hat{H}_{molecule}$ is the Hamiltonian operator and E_n gives the allowed energies.

Likewise, the energy eigenstates of an isolated radiation field may be described by:

$$\hat{H}_{field}\ \phi(X) = E\ \phi(X) \tag{I-9}$$

Such a radiation field may be shown to be analogous to a set of quantized harmonic oscillators[35]. For this system the Hamiltonian operator can be written in analogy to the classical case as[36]:

$$\hat{H}_{field} = \frac{1}{2} \sum_j (\hat{P}_j^{\,2} + \omega_j^{\,2}\ \hat{Q}_j^{\,2} - \hbar\omega_j) \tag{I-10}$$

Where $\hat{P}_j$ and $\hat{Q}_j$ are momentum and position operators, respectively, for the j-th harmonic oscillator.

ϕ may be written as a product of harmonic oscillator wave functions:

$$\phi_{n_1,\, n_2,\, n_3,\, \ldots} = \prod_i \phi_{n_i} \tag{I-11}$$

By using shift operators:

$$\begin{aligned} \hat{A}_j^* &= \frac{1}{2}\left(\hat{Q}_j - \frac{i}{\omega_j}\hat{P}_j\right) \\ \hat{A}_j &= \frac{1}{2}\left(\hat{Q}_j + \frac{i}{\omega_j}\hat{P}_j\right) \end{aligned} \tag{I-12}$$

which have the property of respectively raising and lowering the quantum number of the j-th oscillator by one, the energy levels may be shown to be[34]:

$$E_{n_1,\, n_2,\, n_3 \ldots} = \sum_j n_j\, \omega_j\, \hbar \tag{I-13}$$

In the case of the radiation field n_j gives the number of photons present with energy $\hbar\omega_j$. $\hat{A}_j^*$ creates (and $\hat{A}_j$ annihilates) photons with energy $\hbar\omega_j$. The vector potential describing the radiation field at the position of the j-th atom may be written[34]:

$$\hat{A}_j = \sum_j \hat{U}_i\left(C\hat{A}_i + C'\hat{A}_i^*\right) \tag{I-14}$$

where C and C′ depend on i and j and $\hat{U}_i$ gives the direction of polarization of the i-th photon.

As observed, the light-matter interaction responsible for the Raman effect is normally very weak and its effect may be investigated

by time dependent perturbation theory. The interaction Hamiltonian may be formed by analogy to the classical force exerted on a charged particle in an electromagnetic field. When written quantum mechanically, the Hamiltonian is[34]:

$$\hat{H}_{\text{interaction}} = \left[\sum_j K_1(j)\ (\hat{A}_j \cdot \nabla) + K_2(j)\ \hat{A}_j^{\,2}\right] \tag{I-15}$$

where $K_1(j)$ and $K_2(j)$ are constants.

In terms of shift operators:

$$\hat{H}_{\text{interaction}} = \sum_j \sum_\ell \ (C_1 \hat{A}_\ell + C_2 \hat{A}_\ell^{\,*})$$

$$+ \sum_m (d_1 \hat{A}_\ell \hat{A}_m + d_2 \hat{A}_\ell^{\,*} \hat{A}_m^{\,*} + d_3 \hat{A}_\ell \hat{A}_m^{\,*} + d_4 \hat{A}_\ell^{\,*} \hat{A}_m) \tag{I-16}$$

where j sums over all charged particles and 1 and m sum over photon states in the field.

The coefficients C and d have the form[36]:

$$C \sim \exp \pm \left(\frac{i}{\hbar C}\ (\vec{k}_\ell \cdot \vec{r}_j)(\hat{U}_\ell \cdot \vec{\nabla}_j)\right)$$

$$d \sim \left[\exp \frac{i}{\hbar C}\ (\pm \vec{k}_\ell \cdot \vec{r}_j \pm \vec{k}_m \cdot \vec{r}_j)\right] (\hat{U}_\ell \cdot \hat{U}_m) \tag{I-17}$$

Here $\vec{k}_i$ is a vector whose direction specifies the direction of propagation of the i-th photon and whose magnitude gives the energy of this photon. The unit vector $\hat{U}_\ell$ gives the polarization of the ℓ-th state of the field. $\vec{r}_j$ is the position vector of the j-th atom relative to an arbitrary origin.

Without any interaction between the molecule and field the eigenstates of the composite system would be:

$$\Psi(X,t)_{n,n_1,n_2,n_3,\ldots} = \psi_n(X)\phi_{n_1,n_2,n_3}(X)\, e^{-\frac{it}{\hbar}(E_n+E_{n_1}+E_{n_2}+E_{n_3}+\ldots)}$$

$$= \Psi_N\, e^{-i\frac{E_N}{\hbar}t} \qquad \text{(I-18)}$$

When the perturbation is included these states will no longer be eigenstates, but will serve as a basis set for the expansion of the eigenvectors Ψ' of the total Hamiltonian:

$$\hat{H}_{total} = \hat{H}_{molecule} + \hat{H}_{field} + \hat{H}_{interaction} \qquad \text{(I-19)}$$

thus

$$\Psi'(X,t) = \sum_N b_N(t)\, \Psi_N(X)\, e^{-\frac{iE_N t}{\hbar}} \qquad \text{(I-20)}$$

Using the standard methods of time dependent perturbation theory the time rate of change of $b_N(t)$ may be written to different orders of approximation[34]:

$$\dot{b}_j^{(0)}(t) = 0$$

$$\dot{b}_j^{(1)}(t) = -\frac{i}{\hbar}\sum_N b_N^{(0)}(t)\, H_{jN}\, e^{\frac{i(E_j-E_N)t}{\hbar}}$$

$$\dot{b}_j^{(2)}(t) = -\frac{i}{\hbar}\sum_N b_N^{(1)}(t)\, H_{jN}\, e^{\frac{i(E_j-E_N)t}{\hbar}} \qquad \text{(I-21)}$$

$$\text{where } H_{jN} = \langle \Psi_j^* | H_{INT.} | \Psi_N \rangle$$

These equations may be integrated subject to the proper initial conditions to approximate $b_j(t)$ to different orders and give the probability of various transitions. If the system is required to be in a state 0

before the perturbation is applied, the zero-th order conclusion is that it will remain in that state. The first order result predicts that there is a probability of transition per unit time between states 0 and m given by[36]:

$$W_{mo} = \frac{2\pi}{\hbar} H_{mo} H^{*}_{mo} \rho(E) \qquad \text{(I-22)}$$

Where $\rho(E)$ is the density of states as a function of energy. The matrix elements H_{mo} include contributions from the first two terms in Eq. (I-16) which lead to the absorption or emission of one photon. The remaining four terms in Eq. (I-16) describe possible two photon routes between states 0 and m. These processes will be much less probable than the one photon transitions and may be shown to contribute only to Rayleigh scattering[36].

If the second order perturbation equation is used, with the stipulation that no single photon transition be allowed between states 0 and m, a result analogous to equation (I-22) is gotten[36]:

$$W_{mo} = \frac{2\pi}{\hbar} K_{mo} K^{*}_{mo} \rho(E) \qquad \text{(I-23)}$$

Here, however,

$$K_{mo} = \sum_{N} \frac{H_{NO} H_{mN}}{E_o - E_N} \qquad \text{(I-24)}$$

where the summation covers all states of the system. In this case only the contributions to the matrix elements from the first two terms of Eq. (I-16) need be considered. Again, this second order result describes a two photon path between states 0 and m. Here the set of states N which are coupled to both 0 and m by non-zero matrix elements serve as

intermediates. Energy is in general not conserved in transitions to these intermediate states and the "absorption" and "emission" steps cannot be time resolved. The intermediate states are thus called "virtual" states. The lifetime for Raman scattering is much shorter ($< 10^{-11}$ sec.) than for fluorescence[37].

If the energy of an absorved photon matches the energy difference between some state of the molecule and the initial state, then energy will be conserved in the transition to N and $E_0 = E_N$. If H_{NO} and H_{mN} are non-zero for the above states then this perturbation method clearly fails. A more general perturbation method predicts a resonance enhancement of Raman scattering under these conditions[34].

The results above have been given for a single molecule in a radiation field. Systems which are studied experimentally contain large numbers of molecules. If the interactions among these molecules are considered then a quantum mechanical description becomes extremely difficult. By considering only thermal interactions between molecules, the ratio of the intensity of an anti-Stokes to the corresponding Stokes line can be calculated. In this case the intensity of scattering (either Stokes or anti-Stokes) is the product of the probability of scattering from each molecular state and the population of each state. The ratio of the number of molecules in the state m compared to those in the state 0 is given by the Boltzmann factor[38]:

$$\frac{n_m}{n_o} = e^{-\frac{\Delta E_{mo}}{kT}} \qquad \text{(I-25)}$$

Thus this factor appears in the quantum mechanical result but could not

be expected from the purely classical approach discussed before.

In summary, the quantum mechanical approach explains several features of Raman scattering which do not arise classically. Among these are: 1) The influence of excited molecular states. 2) The short lifetime of scattering. 3) The resonant enhancement of Raman scattering. 4) The Boltzmann factor in anti-Stokes/Stokes intensity ratios.

CHAPTER II

EXPERIMENTAL EQUIPMENT, MATERIALS, AND METHODS

Raman Instrumentation

The computer controlled Raman spectroscopy system used in this study is shown in Figure 6. A Coherent Radiation CR-6 argon ion laser provided the intense, monochromatic, polarized light used to induce Raman scattering. Using this laser several wavelength choices are available between 528.7 nanometers (nm.) and 454.5 nm. Higher output powers may be obtained by using the lines at 514.5 nm. and 488.0 nm. The 488.0 nm. line was chosen for most series of studies because it provided ample incident power with good stability and minimized fluorescence interference, where this was a consideration (see materials section). A narrow bandpass filter was used to transmit light at the laser frequency, while eliminating interference from non-lasing plasma emissions.

Laser powers between 50 and 200 milliwatts (mw.) (measured at the sample) were used to examine the drug and drug-DNA complexes. The laser beam was carefully positioned and focussed inside the sample cell which consisted of a quartz capillary with a flat bottom. The volume of this cell was approximately 10 microliters (µl.), but as little as 2.5 µl. of sample solution could be used without compromising the quality of the resultant spectrum. The sample cell was held in an aluminum block which could be thermostatted by circulating water between $1^{o}C$ and $70^{o}C$. The laser beam entered the bottom of the cell and passed

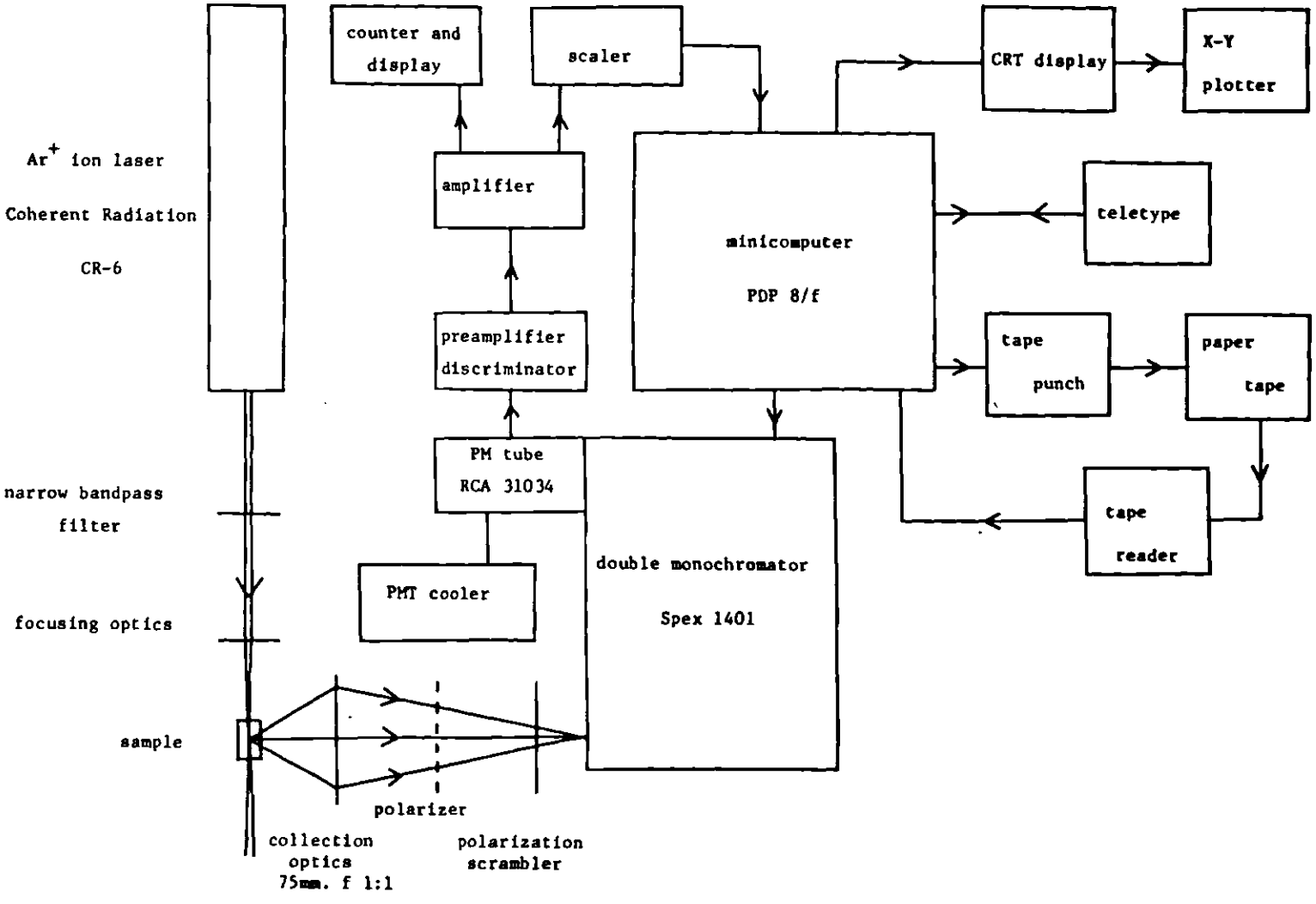

Figure 6. Raman System Diagram.

along the cylindrical axis. The scattered light was collected at 90^{o} from the incident beam, passed through a polarization scrambler, and was focussed on the entrance slit of a Spex 1401 double monochromator. In this device two gratings are used in series to reduce the interference due to the intense light which is unshifted in frequency (due to Rayleigh scattering and incidental reflections). The effective slit width of the spectrometer was 4.5 $cm.^{-1}$. The light signal was detected at the exit slit of the monochromator by a cooled RCA 31034 photomultiplier specially selected for low dark current.

The central component in the electronic portion of the signal path was a Digital Equipment Corp. PDP 8/f computer. This computer served a wide range of functions including: 1) controlling the frequency scanning of the spectrometer, 2) storing the data as a multichannel analyzer, 3) processing the data in specialized ways useful for spectral analysis, and 4) inputting and outputting the data.

During the recording of a spectrum pulses from the photomultiplier were amplified and then counted digitally by a scaler. The computer controlled the time period during which the scaler counted, stored the resulting number, and cleared the scaler. The frequency selected by the spectrometer was then incremented slightly by a servo motor drive controlled by a pulse train from the computer. This process was repeated until the required amount of data was acquired. The programming allowed automatic multiple scanning of a frequency interval in order to minimize the influence of slowly varying factors on the recorded spectrum. This capability was also used to test the accuracy of the computer control over the spectrometer scanning. The wavelength

indicator of the spectrometer was monitored visually during 25 multiple scanning cycles. Variations of less than 0.2 $cm.^{-1}$ were observed in the end points of all cycles. No cumulative errors were noted.

The parameters discussed above, such as the number of data points, the frequency increment between channels (by which the computer determined the number of pulses to send to the spectrometer), the counting time per channel, and the starting frequency, were provided to the computer through an initial dialogue before each run. Immediately prior to recording a spectrum the system scanned slowly across the frequency region containing the chosen laser line. By recording the intensity profile of the heavily attenuated laser line its center could be found very accurately. This process also confirmed that the laser was set on the proper line (sometimes a problem for weak lines close together in frequency) and was tuned properly for stable operation. The frequency shift of each channel in a spectrum was then determined by how far the spectrometer had been scanned from the center of the exciting line. This process eliminated a dependence on the exact calibration of the spectrometer since only frequency shifts are of interest in Raman spectroscopy.

During the recording of data, a partial spectrum was displayed on a CRT scope. The scale could be adjusted to allow evaluation of fine and gross features of the spectrum. The frequency shift associated with observed bands could be determined. In its off-line mode (not simultaneous with data taking) the computer offered more powerful analysis capabilities. These included the ability to subtract arbitrary linear baselines from whole spectra, find the integrated intensities of

bands, and add or subtract two whole spectra channel-by channel in arbitrary proportions. A wide range of input/output devices were interfaced to the computer. In addition to the CRT display, data could be graphed on an X-Y plotter, listed on a teletype, or punched by a high speed paper tape device for later use with the paper tape reader.

Sample Materials

Netropsin samples were generously provided by N. Belcher, Pfizer Inc.; L. Ninet, Rhone Poulenc; F. Aracamone, Farmitalia; and E. L. Patterson, Lederle Laboratories. Distamycin A was obtained from Boehringer Mannheim Inc. Netropsin samples, available in both sulfate and hydrochloride forms, were purified by repeated recrystallization into the sulfate form. Various concentrations of the drug were used up to its solubility limit. At room temperature this was about 0.7 mg/ml. The distamycin A samples required no purification to obtain high quality spectra. Because the solubility of distamycin A is much greater than netropsin, concentrations up to 2.5 mg/ml could be used. Spectra were obtained from 100 cm^{-1} to 2000 cm^{-1}.

Care was taken to minimize the length of time the samples were irradiated and the laser powers used. Precautions were taken to ensure that the exposure of the sample to laser light did not lead to experimental artifacts. Features of the UV spectra of the drugs were used to monitor possible drug changes due to irradiation. Because of their importance, these tests are described in detail below.

Netropsin and distamycin A have two absorption peaks in the ultraviolet (Figure 7). (In netropsin these occur at 235 nm. and 295 nm.

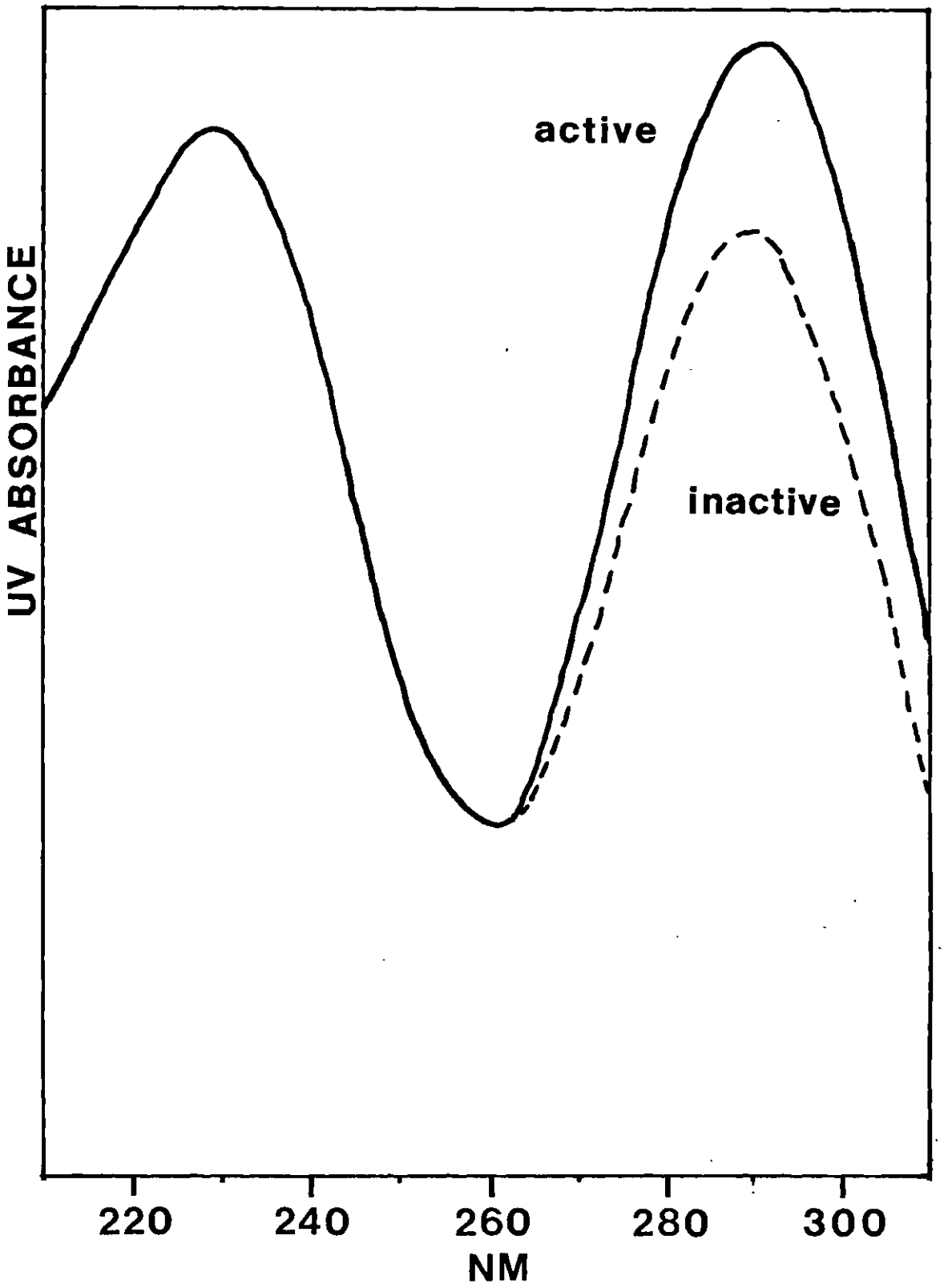

Figure 7. Ultraviolet Absorption Spectra of Netropsin and Distamycin A.

and in distamycin A at 237 nm. and 303 nm.) The lower wavelength absorptions do not change significantly when the drugs bind to DNA. The higher wavelength absorptions shift upward in wavelength by approximately 30 nm. upon DNA binding and have been assigned to sets of coupled N-methyl pyrrole rings[1]. A correlation[22] has been noted between a particular characteristic of the UV spectrum of unbound netropsin and its ability to subsequently bind to DNA. When the UV absorbance ratio A_{295}/A_{235} is found to approach 1.15, the netropsin sample binds strongly to DNA under proper conditions. However, as this ratio falls below 1.00 (as occurs in a sample left at room temperature for several days) the independently measured binding has been found to decrease greatly. Presumably the mechanism of inactivation involves changes which influence the coupled pyrrole rings. A similar monitoring was used for distamycin samples. Tests using this criterion showed that laser irradiation did not significantly increase the normal slow decay process. Samples of drugs recovered after actual runs showed no significant differences in this UV characteristic. Raman spectra obtained at 25°C and 1°C were not significantly different.

The drugs were dissolved in a 3-4 mM sodium chloride solution at pH = 6.0-7.0. Calf thymus DNA, obtained from Sigma Chemical Co., was chloroform extracted and sonicated, then extensively dialysed with 1.0 mM NaCl. It was rotoevaporated to dryness and redissolved with double distilled water to a final concentration of 6.0 mg/ml. The sodium ion concentration was approximately 3 mM. The polymer poly d(A-T)·poly d(A-T) (gift of R. D. Wells, University of Wisconsin) was treated in a manner similar to the calf thymus DNA and employed at a concentration of 4 mg/ml. Drug-DNA complexes were formed by mixing concentrated solutions

of drug and DNA in a molar ratio of approximately 20 base pairs of DNA per drug molecule. The Raman spectra of each binding mixture were reproduced in three separate experiments. Pyrrole, N-methylpyrrole, and N-methylpyrrole-2-carboxaldehyde were obtained from Aldrich Chemical Co. In order to eliminate strong fluorescence interference, each was vacuum distilled immediately prior to its spectroscopic use. The samples were protected from oxidation by a dry nitrogen atmosphere while their spectra were obtained.

Methods of Analysis

The two different major types of analysis used in this study are described below. The first of these involved processing raw spectral data into a form in which relevant comparisons could be made. The second analysis problem was more elaborate and consisted of relating observed Raman bands of the drugs to vibrational motions of these molecules.

Analyses of binding experiments required careful comparisons of the Raman bands of the drugs in the presence and absence of DNA bands. This was greatly facilitated by the digital data storage and fast data processing afforded by the on line computer system. Particularly useful was the ability to subtract proportions of one spectrum from another channel-by-channel. For two spectra, each containing 1024 data points, this process required less than 5 seconds.

This technique was used to normalize the various spectra of each binding experiment (i.e. drug alone, DNA alone and drug+DNA). Varying amounts of a standard buffer spectrum were subtracted from each data spectrum until the water band (1645 cm^{-1}) was removed

completely. (This is illustrated in Figure 8). The required amount of the standard buffer spectrum was then indicative of the intensity of the Raman scattering of the water. The intensity of the water scattering in turn measures the combined effect of experimental factors, such as, laser power, optical alignment, slit width, and counting time. Thus the intensity of the various spectra could be corrected for variations of all these factors between runs. The observed intensity of the drug bands depdnds in addition on the concentration of the drug in each sample. This final factor in the normalization was calculated from ultraviolet absorbance data.

To obtain the bound drug spectrum it was necessary to remove the bands due to DNA and buffer from the spectrum of drug+DNA+buffer. This was done by a two step process. Fractions of the standard buffer spectrum were separately subtracted from the spectrum of the drug-DNA mixture and unbound DNA. Proportions of the resultant spectrum of the unbound DNA were then subtracted from the resultant drug-DNA spectrum until the DNA bands were removed. The latter procedure assumed that spectral differences between unbound and partially bound DNA were negligible. This is strictly correct for DNA bands unaffected by drug binding. It should also be approximately correct for other DNA bands, given the 20 to 1 molar ratio of nucleotide pairs to drug. Additionally, only those DNA bands which overlap drug bands have the potential for significantly distorting the resultant spectrum. Tests can be made for the validity of this procedure. One such test is the ability to accurately remove all major DNA bands by a single subtraction of a proportion of the resultant unbound DNA spectrum without distorting

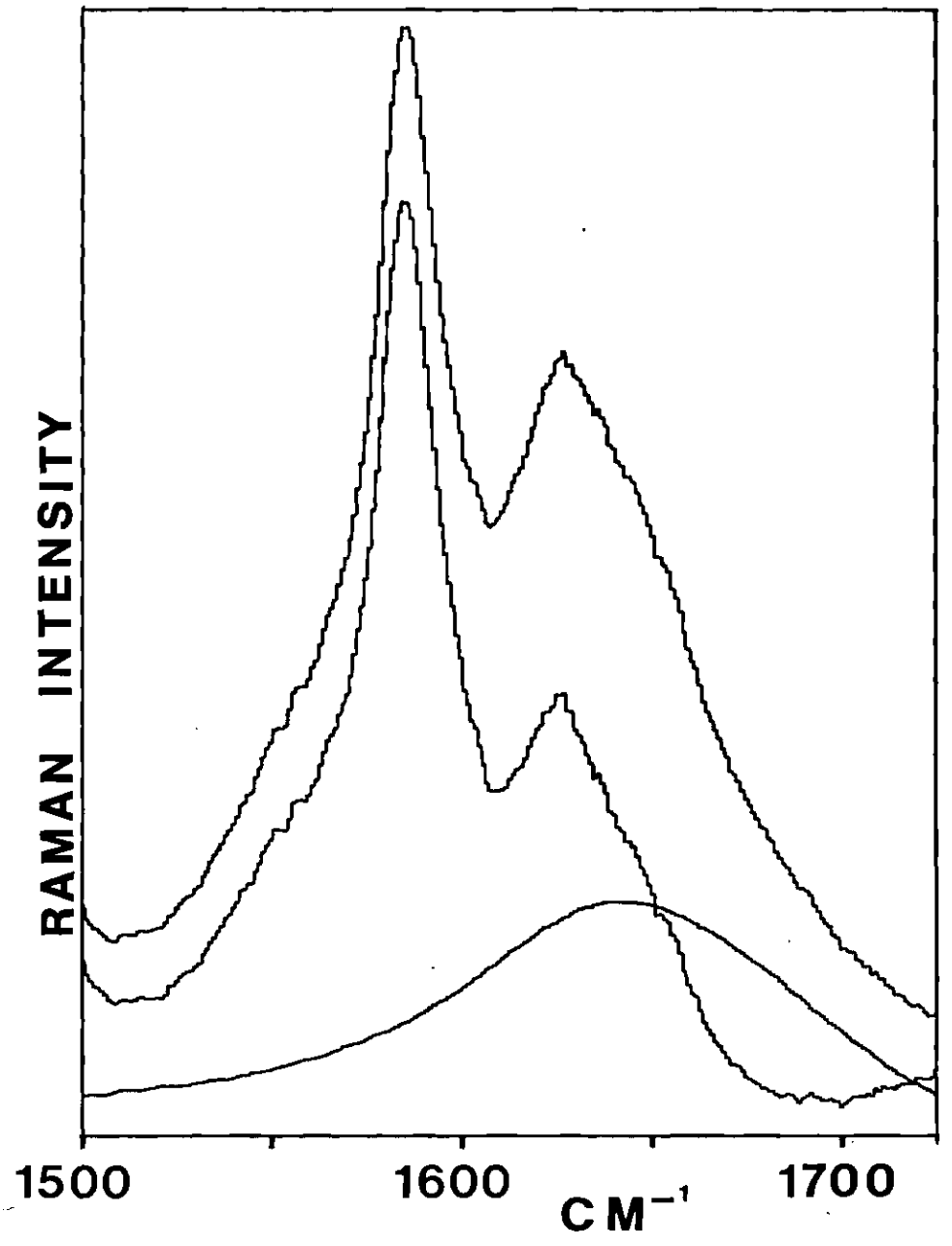

Figure 8. Spectral Subtraction of the 1645 cm^{-1} Water Band.

the background of the final spectrum. Secondly, there should be no correlation between observed changes in the bound vs. free drug spectra and the positions of DNA bands. Figure 13 shows that the background of the bound and free distamycin spectra are undistorted and follow each other. Changes between the bound and free drug spectra do not show a strong correlation with the positions of DNA bands.

In order to draw conclusions about binding changes by Raman spectroscopy it is necessary to assign the observed Raman bands to the modes of vibration of the molecule from which they arise. This assignment problem is generally complex for molecules the size of these drugs. When completed, however, each Raman band serves as a probe of what is happening to specific parts of the drug, making detailed conclusions possible. Several techniques of increasing complexity were utilized to make assignments.

Certain chemical groups within a large molecule have vibrational modes which are isolated by frequency and symmetry from the motions of the rest of the molecule[39,40]. Thus these frequencies are approximately characteristic of the group alone and may be transferrable to different molecules. This approach was used in our work to give approximate frequencies for bands from the methyl and amide groups as shown in Table 2.

In order to assign the bands resulting from less localized modes we investigated spectroscopically several compounds as models for parts of the drugs. For example, pyrrole, N-methylpyrrole, and N-methyl pyrrole-2-carboxaldehyde were used to model the pyrrole rings and surrounding structures of the drugs. Some empirical correlations were possible between these spectra on the basis of chemical similarities and differences of the sample molecules. However, this method was not

Table 2. Raman Group Frequencies

methyl rock	1000-1100 cm-1
methyl symmetric bend	1370-1390 cm-1
methyl antisymmetric bend	1440-1460 cm-1
amide I C=O stretch	1650-1660 cm-1
amide II N-H bend	1540-1565 cm-1
amide III N-H bend & C-N stretch	1250-1300 cm-1
amide IV O=C-N bend	600- 775 cm-1

found to be satisfactory since closely spaced Raman bands could not be reliably distinguished as they shifted about. This led to the use of normal coordinate analysis (NCA) to actually predict the frequencies of these model compounds. By comparing the calculated frequencies and normal modes for these molecules with their spectra many changes could be confidently followed. Very good predictions were obtained for the direction and magnitude of frequency shifts observed between pyrrole and its derivatives. Further discussion of this will be given in "Results."

On the basis of this success, the NCA method was used to examine a fragment common to the drug molecules (shown in Figure 3c). Due to the extreme importance of NCA to this investigation, the technique is described at length in the following chapter.

CHAPTER III

NORMAL COORDINATE CALCULATIONS

Basic Theory

The general problem of predicting the vibrational spectrum (IR and Raman) of a molecule is presently undertaken in distinct parts. The techniques range from purely classical to quantum mechanical. Vibrational frequencies and normal modes are calculated by the specialized classical methods appropriate for small oscillations. Where molecular symmetry is present, group theoretic methods may readily show which of the calculated modes are Raman and/or IR active. This much may be achieved without recourse to any quantum mechanical calculations. In addition, for small molecules (and localized portions of larger ones) the intensities of vibrational bands and the magnitudes of interatomic forces may be calculated ab initio.

The goal of the present investigation is to assign experimentally observed Raman bands from complex, non-symmetric drug molecules to the vibrational modes from which they arise. This will be undertaken by the classical calculations, mentioned above, which are called normal coordinate analysis (NCA).

In NCA molecules are modeled by point atomic masses connected by massless Hooke's Law springs. (For some investigations anharmonic force constants are considered.) The point masses are assumed to oscillate freely with very small amplitudes about positions of stable equilibrium. Under these conditions only fundamental frequencies are

excited and functions need be considered only to lowest order in atomic displacements[41]. Newton's equations of motion in the Lagrangian formulation are employed to calculate the frequencies and normal modes of vibration. Although several specialized coordinate systems and methods of calculation may be used in this problem, the basic theory remains the same. This is illustrated below for a system of n atoms using a cartesian coordinate system ($S_1 . . . . . S_{3n}$) which measures the deviations from the equilibrium positions of the atoms ($X_{1_o} . . . . X_{3n_o}$). These coordinates are related to general cartesian coordinates X_i by:

$$X_i = X_{io} + S_i \text{ For } i = 1 \text{ to } 3n \qquad \text{(III-1)}$$

In this system the potential energy may be expanded about the equilibrium configuration of the molecule as:

$$2V(X_1 \ldots . X_{3n}) = 2V(X_{1_o} \ldots . X_{3n_o}) + 2 \sum_{i=1}^{3n} \left(\frac{\partial V}{\partial X_i}\right)_o S_i + \sum_{j,k}^{3n} \left(\frac{\partial^2 V}{\partial X_j \partial X_k}\right)_o S_j S_k$$

$$+ \text{higher order terms} \qquad \text{(III-2)}$$

The constant first term may be made to vanish by choosing the potential energy to be zero at equilibrium. Since the derivatives in the second term represent components of force, they must all be zero at equilibrium. Because of the infinitesimal nature of atomic displacements, only the first non-vanishing term will be important. Thus the form of the potential energy is:

$$2V(S_1 \ldots S_{3n}) = \sum_{j,k}^{3n} V_{jk} S_j S_k \quad \text{where} \quad V_{jk} = \left(\frac{\partial^2 V}{\partial X_j \partial X_k}\right)_o \qquad \text{(III-3)}$$

In cartesian coordinates the kinetic energy is particularly simple:

$$2T(S_1,\ldots,S_{3n}) = \sum_{i=1}^{3n} m_i \dot{S}_i^2 \qquad \text{(III-4)}$$

In this sum the mass of the ℓ-th atom occurs three times as $i = 3\ell - 2$, $3\ell - 1$, and 3ℓ.

Since V is solely a function of atomic displacements and T is a function of velocities only, Newton's equations may be written:

$$\frac{d}{dt}\left(\frac{\partial T}{\partial \dot{S}_i}\right) + \frac{\partial V}{\partial S_i} = 0 \qquad \text{(III-5)}$$

Upon substitution of T and V a system of 3n linear differential equations with constant coefficients results. These equations which have the form:

$$m_i \ddot{S}_i + \sum_{j=1}^{3n} V_{ij} S_j = 0 \qquad \text{(III-6)}$$

are known to have 3n oscillatory solutions[41]. If the k-th solution is assumed to have the form:

$$S_i = A_{ik} \sin(\sqrt{\lambda_k}t + \alpha) \qquad \text{(III-7)}$$

then, the differential equations are placed by a set of 3n coupled algebraic equations called the secular equations.

$$\sum_{j=1}^{3n} (V_{ij} A_{jk} - A_{ik} m_i \lambda_j \delta_{jk}) = 0$$

or (III-8)

$$\sum_{j=1}^{3n} V_{ij} A_{jk} = A_{ik} m_i \lambda_k$$

A_{jk} is the amplitude of oscillation for the j-th coordinate in the k-th solution. These oscillatory amplitudes are the unknowns in this system of equations. However, solutions for the system will be possible only when λ_k takes on certain discrete values called eigenvalues. The frequency of an oscillation described by equation (III-7) is related to λ_k by[41]:

$$\nu_k = \frac{1}{2\pi} \sqrt{\lambda_k} \qquad \text{(III-9)}$$

Thus a set of discrete vibrational frequencies ν_k will result, each with a corresponding set of amplitudes A_{jk} for the j coordinates.

The solution of the secular equations may be completed by well known algebraic methods. However, for problems of sufficient complexity to warrant the use of computers, a matrix formulation is indicated. In this method the elements V_{ij} (see Eq.(III-3)) are assembled into a 3nx3n matrix $\mathbf{V}$ which is real and symmetric. The eigenvalues $\lambda_1 \ldots \lambda_{3n}$ form the diagonal elements of an otherwise null matrix $\boldsymbol{\lambda}$. The A's form a 3nx3n matrix $\mathbf{A}$ in which the k-th column of A_{jk}'s gives the amplitudes for a distinct eigenvalue λ_k. The n masses each appear three times down the diagonal of an otherwise null matrix $\mathbf{M}$. In this notation the secular equations may be written as:

$$\mathbf{VA} = \mathbf{MA}\boldsymbol{\lambda} \qquad \text{(III-10)}$$

Upon multiplication from the left by $\mathbf{A}'$ (the transpose of $\mathbf{A}$) this gives:

$$\mathbf{A}'\mathbf{VA} = \mathbf{A}'\mathbf{MA}\boldsymbol{\lambda} \qquad \text{(III-11)}$$

In Appendix C it is shown that for the case of distinct eigenvalues:

$$\mathbf{A'MA=1} \tag{III-12}$$

(This result may also be shown to be valid when degeneracy occurs).

Equations (III-11) and (III-12) may be written:

$$\mathbf{A'VA=\lambda}$$
$$\mathbf{A'MA=1} \tag{III-13}$$

Thus a matrix $\mathbf{A}$ may be found which diagonalizes $\mathbf{V}$ by a congruent transformation to a diagonal matrix whose non-zero elements are the eigenvalues. This same transformation also diagonalizes $\mathbf{M}$ to the unit matrix. The importance of this result may be seen by considering the transformation to a generalized coordinate system $\boldsymbol{\eta}$ defined by the use of $\mathbf{A}$ as:

$$\mathbf{S=A\eta} \tag{III-14}$$

Here $\mathbf{S}$ and $\boldsymbol{\eta}$ represent column vectors of all the cartesian coordinates S_i of the molecule and the new set of coordinates η_i. In matrix notation the potential energy is given by:

$$\mathbf{2V=S'VS=\eta'A'VA\eta} \tag{III-15}$$

$$\mathbf{2V=\eta'\lambda\eta} \tag{III-16}$$

Also:

$$\mathbf{2T=S'MS=\dot{\eta}'A'MA\dot{\eta}=\dot{\eta}'\dot{\eta}} \tag{III-17}$$

Thus in the coordinate system $\boldsymbol{\eta}$ (called normal coordinates) both energy expressions occur with no cross terms. In effect, the secular equations have been uncoupled by the principal axis transformation generated by $\mathbf{A}$. Each of the normal coordinates η_i may be excited independently of the others, leading to an in phase vibration, generally involving the whole molecule.

With modern computer storage capabilities and efficient numerical methods, very large matrices may be routinely diagonalized. Using the present diagonalization program and computer hardware, matrices up to about 200 x 200 may be diagonalized. This gives the capability of analyzing molecules of up to approximately 70 atoms. For a problem of this complexity, however, a significant expenditure of computer time would be required.

Computational Approaches

The brief theoretical development given above is general for NCA. However, additional considerations lead to variations in the methods of implementing the calculations. Presently two antithetical approaches to NCA calculations are of general research interest. These may be distinguished as an algebraic and a numerical approach. A comparison of these methods will illustrate the advantages of each for particular types of molecules.

In the algebraic approach the problem is developed so as to minimize the task of matrix diagonalization[42]. This is accomplished by the use of very specialized coordinate systems, rather than the cartesian coordinate discussed previously. Recall from equations (III-3)

and (III-4) that while the expression for kinetic energy is simple in cartesian coordinates, the opposite is true for potential energy. The use of the elements $V_{jk} = (\frac{\partial^2 V}{\partial X_j \partial X_k})_o$ to express potential energy has several disadvantages. These force constants are not invariant to rotations of the molecule as a whole and are not easily transferrable from one molecule to another. They do not provide the basis for a physical distinction between the stretching, bend, and twisting of chemical bonds. The expression of the potential energy in terms of meaningful force constants thus requires the use of a set of internal coordinates ζ_i fixed on the molecule, which measures changes in bond lengths, interbond angles, and dihedral angles. In these coordinates the potential energy is given by:

$$2V = \sum_{j,k} F_{jk} \zeta_j \zeta_k$$

or in vector notation: (III-18)

$$2V = \boldsymbol{\zeta}' \mathbf{F} \boldsymbol{\zeta}$$

On diagonal elements F_{ii} represent force constants corresponding to a change of the i-th coordinate. Off diagonal elements reflect the interaction forces between different coordinates. The use of internal coordinates has the additional advantage of eliminating up to six coordinates (five for linear molecules) taken up in a cartesian system by translations and rotations of the center of mass of the molecule.

Such a reduction decreases the size of the matrix which must be diagonalized. Unfortunately, all of this reduction is not usually realized due to another property of internal coordinates. Unlike cartesian coordinates, these internal coordinates are generally not independent. As an example, for the in-plane vibrations of a trigonal molecule a set of six internal coordinates is suggested. These coordinates consist of two sets, each of which contains symmetrically equivalent elements. One set contains three bond length changes and the other contains three changes in interbond angles in the molecular plane. However, four atoms constrained to a plane have only eight degrees of freedom, of which three describe translations and rotations. Thus the six vibrational internal coordinates contain one redundant coordinate, which is in this case one of the angle changes. This can be demonstrated since the three interband angles cannot be independently adjusted. In fact, a redundancy condition may be written:

$$\theta_{12} + \theta_{23} + \theta_{31} = 2 \qquad \text{(III-19)}$$

This equation may be used to eliminate one of the coordinates. More often, however, all internal coordinates are retained until the end of the problem in order to exploit the symmetrical equivalence of these redundant sets. In order to recast the vibrational problem in internal coordinates the kinetic energy must be expressed in this system. This may be accomplished by determining the transformation

between cartesian and internal coordinates. The conformation of the molecule determines the form of the internal coordinates and, therefore, the details of the transformation. Wilson[42] has developed a method of expressing the kinetic energy directly in internal coordinates in terms of an auxiliary matrix such that:

$$2T = \dot{\zeta}' \mathbf{G}^{-1} \dot{\zeta} \qquad \text{(III-20)}$$

The elements of $\mathbf{G}$ depend on atomic masses and positions and all contributions to their algebraic form have been fully cataloged[42]. The solution of the vibrational problem in internal coordinates follows that given for cartesian coordinates.

Where molecular symmetry is present, a much more important simplification of the diagonalization problem may be realized. In fact, the attractiveness of the algebraic method of NCA depends largely on the use of this simplification. Here again, a specialized coordinate system (called symmetry coordinates) is employed to eliminate cross terms in the energy expressions and thereby decouple the secular equations. This process differs in two ways from the previous use of normal coordinates.

First, the use of symmetry coordinates does not eliminate all energy cross terms and uncouple all secular equations. In terms of the matrix diagonalization task, the simplification is described schematically in Figure 9. Non-zero elements occur only in blocks along the diagonal. The coordinates which correspond to these blocks

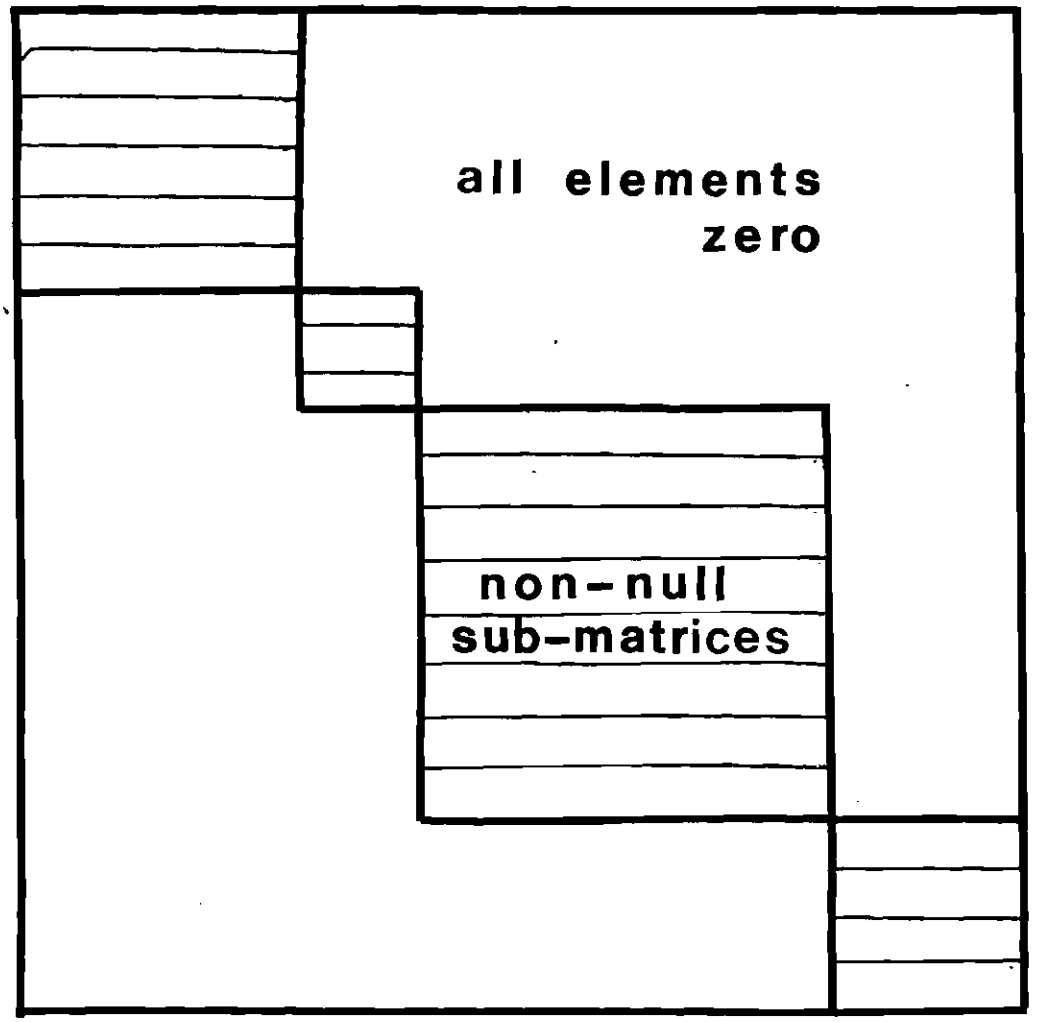

Figure 9. Schematic Diagram of Matrix Diagonalization Problem.

have the same symmetry properties. Elements in the matrix resulting from coordinates of different symmetries are all zero. The diagonalization of the resulting matrix requires only the separate diagonalization of the non-zero submatrices. For original matrices which are large this provides a great savings of computer time and reduces storage requirements.

Symmetry coordinates also differ from normal coordinates in how they are determined. Rather than resulting from the diagonalization process, symmetry coordinates are established, a priori, on the basis of molecular symmetry. Linear combinations of internal coordinates are formed which transform according to the irreducible representations of the molecule's symmetry group. This process may be undertaken in a systematic manner using projection operator techniques. With experience, however, some symmetry coordinates may be arrived at by observation.

The method of NCA used in this study avoids algebraic development in favor of a first principles approach[43]. The necessary transformation between cartesian and internal coordinates is obtained by numerical differentiation. Each internal coordinate ζ_i may be expanded in terms of cartesian coordinates S_j about the molecule equilibrium configuration as:

$$\zeta_i(S_1,S_2,\ldots,S_{3n}) = \zeta_i(S_{1_o},S_{2_o},\ldots S_{3n_o}) + \sum_j \left(\frac{\partial \zeta_i}{\partial S_j}\right)\Big|_o S_j + \text{higher terms} \qquad \text{(III-21)}$$

Both cartesian and internal coordinates may be made zero at equilibrium and only first order terms need be retained:

$$\zeta_i(S_1,S_2,\ldots S_{3n}) = \sum_j \left(\frac{\partial \zeta_i}{\partial S_j}\right)\Big|_o S_j = \sum_j P_{ij}S_j \qquad \text{(III-22)}$$

The value of each internal coordinate can be calculated in terms of the cartesian coordinates of the involved atoms. This may be done in general for each of the categories of internal coordinates (stretches, bends, wags, and torsions) using simple manipulations of vectors. Again these calculations are simplified since they need be made only to first order in cartesian displacements. By making small increments and decrements in each cartesian coordinate, in turn, and calculating the resultant values of the internal coordinates, one can numerically approximate the derivatives:

$$P_{ij} = \left(\frac{\partial \zeta_i}{\partial S_j}\right)\Big|_o \qquad \text{(III-23)}$$

by:

$$P_{ij} = \frac{\zeta_i(S_1,\ldots,S_j+\Delta,\ldots,S_{3n}) - \zeta_i(S_1,\ldots,S_j-\Delta,\ldots,S_{3n})}{2\Delta} \qquad \text{(III-24)}$$

When this procedure is repeated for each internal coordinate a complete table of elements P_{ij} will be determined.

Using these P_{ij} the usual force constants $F_{\ell m}$ appropriate for

internal coordinates are numerically transformed for use in the cartesian system. From Eq. (III-18) the potential energy may be written in internal coordinates as:

$$2V = \sum_{\ell,m} F_{\ell,m}\, \zeta_\ell\, \zeta_m \qquad \text{(III-25)}$$

Using the transformation to cartesian coordinates (Eq.III-21) this gives:

$$2V = \sum_{j,k} \left[\sum_{\ell,m} F_{\ell,m}\, P_{\ell j}\, P_{mk} \right] S_j S_k \qquad \text{(III-26)}$$

Comparing this result to Eq.(III-3) it can be seen that the desired transformation consists of:

$$V_{jk} = \sum_{\ell,m} F_{\ell,m}\, P_{\ell j}\, P_{mk} \qquad \text{(III-27)}$$

The only additional transformation employed in this approach is to mass weighted cartesian coordinates defined by:

$$q_i = \sqrt{m_i}\, S_i \qquad \text{(III-28)}$$

In this coordinate system the kinetic energy matrix is simply the unit matrix. The potential energy matrix elements W_{jk} in the mass weighted system are related to V_{jk} by:

$$W_{jk} = \frac{V_{jk}}{\sqrt{m_j m_k}} \qquad \text{(III-29)}$$

The secular equations now have the form[41]:

$$\mathbf{WA = A\lambda} \qquad \text{(III-30)}$$

and the solution is analogous to that given above. After the vibrational

problem has been solved the genuine vibrations may be distinguished from modes which consist of linear combinations of translations and rotations of the entire molecule. The non-vibrational modes can be immediately distinguished by their zero frequencies.

In summary, the algebraic approach to NCA can greatly reduce the matrix diagonalization difficulty for molecules with significant symmetry. In polymers, for example, this approach may be essential in making the NCA possible. The price paid for these advantages is the additional difficulty of transformations among multiple coordinate systems. This consists mainly of the evaluation of the $\mathbf{G}^{-1}$ matrix elements and the construction of symmetry coordinates. In addition, where non-independent coordinates are used, redundancy conditions must be determined. For complex molecules, particularly those including rings, the difficulty of obtaining and verifying these conditions may cause subtle errors in the calculations which follow.

Because it avoids all these difficulties, the numerical approach is indicated unless symmetry factoring is necessity. This method takes maximum advantage of modern computing capabilities to eliminate time consuming algebra.

When the vibrational problem has been solved (by either procedure above) the relative displacements of each atom may be plotted for each normal mode. For complex molecules, however, this presents a rather confusing picture and more efficient methods are used to characterize the normal mode. A standard approach is to calculate the potential energy distribution (PED) for each normal mode. This calculation is described below as used with the numerical approach. When the

algebraic approach is used this calculation is analogous, but somewhat simpler.

If only the single normal mode η_k (corresponding to eigenvalue λ_k and frequency ν_k) is excited with an arbitrary amplitude η_o, then from equation (III-14):

$$S_i = \sum_{j=1}^{3n} A_{ij}\, \eta_j = \sum_{j=1}^{3n} A_{ij}\, \eta_o\, \delta_{jk} = A_{ik}\, \eta_o \qquad \text{(III-31)}$$

The total potential energy is given by:

$$2V = \sum_{i,j} \left[\sum_{\ell,m} F_{\ell m}\, P_{\ell i}\, P_{mj} \right] \eta_o A_{ik}\, \eta_o\, A_{jk} \qquad \text{(III-32)}$$

$$V = \sum_{\ell,m} \frac{1}{2} F_{\ell m}\, \eta_o^{\,2} \sum_{i,j} P_{\ell i}\, P_{mj}\, A_{ik}\, A_{jk} \qquad \text{(III-33)}$$

Thus each term:

$$\frac{1}{2} F_{\ell m}\, \eta_o^{\,2} \sum_{ij} P_{\ell i}\, P_{mj}\, A_{ik}\, A_{jk} \qquad \text{(III-34)}$$

represents the potential energy which goes with the force constant $F_{\ell m}$.

By dividing the potential energy associated with each force constant by the total potential energy, one obtains the fractional distribution of potential energy among the force constants. Force constants often occur in symmetrically equivalent sets and, therefore, the PED among different sets rather than individual force constants is utilized. This is done separately for each normal mode and the results characterize the vibrational motion occurring in each normal mode.

While the PED is a valuable physical way to describe normal modes, phase information is suppressed due to the scalar nature of energy.

For example, the potential energy would be distributed similiarly in the two vibrational modes of a linear triatomic molecule shown in Figure 5. Since these two modes differ greatly in their Raman intensity, it is necessary to distinguish clearly between two such calculated modes. This is accomplished in this study by the following simple method illustrated in two dimensions in Figure 10. Vectors were formed which give the separations between pairs of atoms. The changes in these vectors were calculated when a single normal mode was excited with arbitrary amplitude. By calculating the component of $\Delta\vec{V}$ parallel to the original vector $\vec{V}_o$ the direction and amount of bond stretch was found for bonded pairs of atoms. This same method was applied to non-bonded atom pairs to determine whether these atoms were moving closer together or further apart during a normal vibration. The component of $\Delta\vec{V}$ perpendicular to $\vec{V}_o$ gives a measure of the twisting of the bond (or the line connecting non-bonded atoms). No distinction is made among twists which arise from bends, wags, or torsions. This method could be extended in several ways to give more specific information. Generally, however, this additional information is available from the PED.

Force Fields

The NCA calculations described above are straight forward and may be performed accurately. The data required include the atomic positions and masses and the sets of force constants $F_{\ell m}$ (where ℓ and m indicate internal coordinates). Together this set of constants is called a force field. Masses of the predominant isotope of each atom are employed. Atomic positions may be calculated from the molecule's

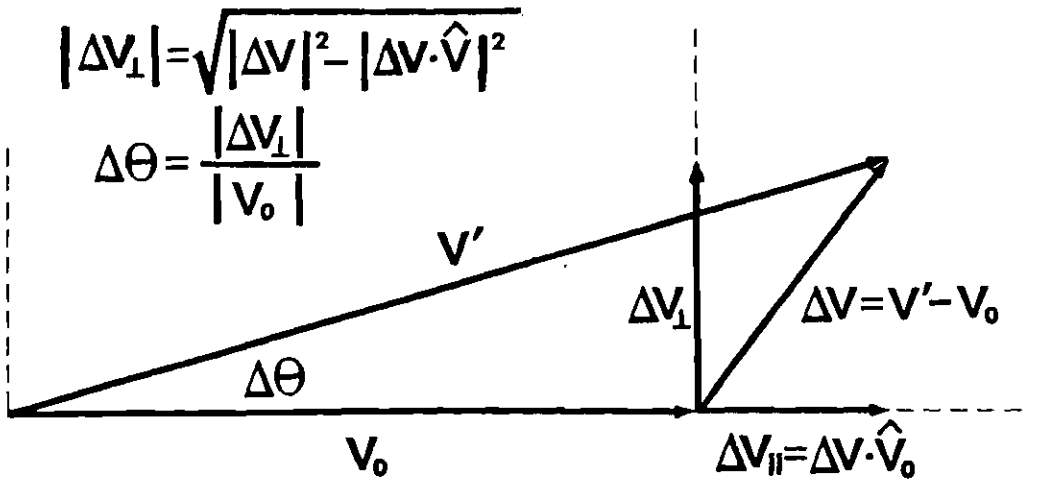

Figure 10. Characterization of Bond Changes as Bends and Stretches

conformation and bond lengths. If this information is unavailable from X-ray or microwave studies then approximate bond lengths and angles may be transferred from similar molecules. The errors caused by this are not usually serious. Knowing a physically realistic force field is the key to any NCA. Force constants for individual bonds are not usually transferable between molecules. They do have validity when viewed as a set which determines the vibrational motion of a group of connected atoms. The on-diagonal force constants F_{jj} are always positive and have values of about 2-10 millidynes/Å for bends[42]. This is generally at least an order of magnitude larger than the off-diagonal constants which reflect the interactions between changes in different internal coordinates. Variations in one internal coordinate may increase or decrease the flexibility of adjacent bonds. Thus, these interaction constants may be positive or negative. For internal coordinates which are widely separated spacially, these constants are often found to be very small and are neglected in an approximation called a partial valence force field. Such a force field is determined from an initial set of force constants by an iterative procedure. The force constants are varied until the difference between the calculated and experimental frequencies is minimized. For this problem to be well determined the number of available experimental frequencies must exceed the number of force constants to be adjusted. Several expedients are used to guarantee this. Where possible, chemical variants of the molecule of interest are studied, in which changes such as methylation and deuteration have been made. These alterations are designed to change the inertial characteristics of the

molecule, but not the interatomic forces. This in effect gives more experimental frequencies without introducing new unknown force constants. Some groups of force constants (many interaction constants, for example) may be set to zero or to another fixed value on physical grounds or from experience with similar molecules. These force constants are not varied in the iteration process. Other force constants which are symmetrically related, may be required to remain equal to each other as they are varied.

Partial valence force fields determined in this way were available for several subunits of netropsin and distamycin, including the pyrrole rings[44] and the peptide group[45]. These force fields were first used to test the computer program. In this process it was discovered that subtle differences may exist among force fields, depending on the computational approach used to develop them. For example, the implicit choices for the positive direction of internal coordinates differ among different programs. This causes no problems in the on-diagonal energy terms since they depend only on the square of a single internal coordinate. However, the interaction energies have the form $\frac{1}{2} F_{\ell,m}\zeta_\ell\zeta_m$ and may therefore be changed in sign by a change in internal coordinate definition. Discrepancies of this kind may be found by comparing the implicit internal coordinate definitions in each program. Corrections may be made by reversing the sign of some of the interaction constants.

Another modification was found necessary in order to use certain force fields with this numerical NCA program. When using the algebraic NCA method, force constants may be defined in relation to symmetry coordinates which are linear combinations of the internal coordinates. For example, in the case of torsion about the C = C bond in ethylene,

four separate torsional angles occur. These are the dihedral angles:

$$\theta_{12}: H_1 - C = C - H_2$$

$$\theta_{23}: H_3 - C = C - H_2$$

$$\theta_{14}: H_1 - C = C - H_4$$

$$\theta_{34}: H_3 - C = C - H_4$$

The restoring force for this torsion may be defined (by the Fukushima convention[46]) in relation to a single internal-rotation symmetry coordinate:

$$\theta = \frac{\theta_{12} + \theta_{23} + \theta_{14} + \theta_{34}}{4}$$

The positive sign is taken for the coordinates when the C-H bond nearer the observer is rotated clockwise relative to the farther bond. The potential energy for the torsion is then given by:

$$V = \frac{1}{2} K\theta^2 = \frac{1}{2} K \left[\frac{\theta_{12} + \theta_{23} + \theta_{14} + \theta_{34}}{4} \right]^2$$

$$V = \frac{1}{2}\frac{K}{16}\theta_{12}^2 + \frac{1}{2}\frac{K}{16}\theta_{23}^2 + \frac{1}{2}\frac{K}{16}\theta_{14}^2 + \frac{1}{2}\frac{K}{16}\theta_{34}^2$$

$$+ \frac{1}{2}\frac{K}{8}\theta_{12}\theta_{23} + \frac{1}{2}\frac{K}{8}\theta_{12}\theta_{14} + \frac{1}{2}\frac{K}{8}\theta_{12}\theta_{34}$$

$$+ \frac{1}{2}\frac{K}{8}\theta_{23}\theta_{14} + \frac{1}{2}\frac{K}{8}\theta_{23}\theta_{34} + \frac{1}{2}\frac{K}{8}\theta_{14}\theta_{34}$$

Because of cross terms, a single diagonal torsional force constant K defined for a symmetry coordinate, gives rise to both diagonal and off-diagonal energy terms. Thus when using the numerical NCA program ten

separate force constants must be entered. Four of these are on-diagonal constants equal to $\frac{K}{16}$ which go with the four torsional internal coordinates. The other six are equal to $\frac{K}{8}$ and are interaction constants between the four torsions. (It should be noted that in this case the interaction constants are twice as large as the on-diagonal force constants and more interaction constants occur. This enhanced importance of interaction constants is physically reasonable in the case of bond torsions. The internal torsional coordinates used in this study must vary cooperatively in order for a true torsion to occur.)

In general, if an internal-rotation coordinate is a sum of dihedral angles, then n diagonal force constants $\frac{K}{n^2}$ and $\frac{n(n-1)}{2}$ interaction constants $\frac{2K}{n^2}$ arise from the single constant K associated with the symmetry coordinate.

This implies that simple, but significant modifications are necessary to transform force fields for use with differing NCA programs.

CHAPTER IV

RESULTS AND DISCUSSION

Normal Coordinate Calculations

Once the modifications described in the previous chapter were complete the vibrational frequencies were calculated for pyrrole, N-methylpyrrole and N-methylacetamide. The values obtained were within 1 cm^{-1} of those frequencies previously reported for these molecules[44,45]. The earlier studies had used programs employing the algebraic approach to develop these force fields. This confirmed that widely differing calculational approaches give similar results.

This program was then used to calculate the frequencies and normal modes for several model systems related to the drug molecules. For this purpose composite force constant sets were obtained by combining force fields for smaller molecular subunits. Each of these component force fields successfully predicts the vibrational behavior of a portion of the model system. Thus the composite force constant set is expected to be the best available predictor of the frequencies and modes of the whole molecule. The discrepancies between calculated and observed frequencies are expected to be somewhat greater using such a composite force field. For purposes of making spectral assignments, however, exact frequencies are not the main requirement. Instead, a method is needed to dependably predict the direction and approximate magnitude of frequency shifts in the Raman bands between related molecules. Together with other information (such as, the approximate

relative intensities of Raman bands due to different types of modes) this method allows one to make confident assignments using all available information about similar molecules.

This is illustrated in Table 3 for the case of pyrrole, N-methylpyrrole and N-methylpyrrole-2-carboxaldehyde. The frequencies and normal modes of the latter molecule were calculated by interfacing force constant sets for N-methylpyrrole and the carboxaldehyde group[47]. Modes which do not involve motions of the added group (for example, ring hydrogen out of plane bending and methyl rocking and bending) are calculated and observed to change only slightly in frequency. Large frequency shifts are correctly predicted for ring in plane bend and stretch modes which are strongly affected by the addition of the methyl and carboxaldehyde groups. The PEDS are used to follow similar modes among the three molecules. While empirical frequency correlations may suffice for following modes which maintain very similar frequencies in different molecules, this may be very misleading at times due to coincidental frequency matches. If a frequency shifts by 40 cm^{-1} or more in a region where lines occur close together, correlations are often impossible without some additional information. The high correlation between calculated and observed frequency shifts comfirms the usefulness of NCA as a source of this needed information.

On the basis of this success, the spectrum of a larger fragment of the drugs was calculated. This fragment was chosen from the chromophore region common to the central portions of both drugs. Because of the great similarity in Raman spectra of netropsin and distamycin, (described below) this common region is suggested for investigation.

Table 3. Frequency Correlations Between Pyrrole and Two Derivatives

Note: The ν_{OBS} values listed under each molecule are experimental frequencies. $\Delta\nu_{OBS}$ and $\Delta\nu_{CALC}$ are the observed and calculated frequency shifts between molecules for bands assigned to common vibrational modes. Frequencies are given in cm^{-1}. All vibrational modes are Raman active. Except for those noted by (*t*), all bands were observed by us. The two additional frequencies are from studies of Scott[14].

Pyrrole			N-Methyl Pyrrole			N-Methyl Pyrrole-2-Carboxaldehyde	
ν_{OBS}	$\Delta\nu_{OBS}$	$\Delta\nu_{CALC}$	ν_{OBS}	$\Delta\nu_{OBS}$	$\Delta\nu_{CALC}$	ν_{OBS}	Assignment
601[t]	9	10	610	0	-7	610	C=C Torsion
			667	31	35	698	Methyl stretch
826[t]	-3	-1	823	3	2	826	Ring H out of plane bend
876	2	2	878	10	25	888	Ring in plane bend
			971	55	47	1026	C-C stretch + Ring H in plane bend
			1063	-7	-5	1056	Methyl rock
1148	-56	-56	1092	0	12	1092	Ring H in plane bend
1387	-1	0	1386	-12	8	1370	Ring stretch
1424	-38	-31	1386	-1	5	1387	N-C stretch
			1422	-6	0	1416	Methyl bend
1532	-17	-10	1512	40	30	1522	C=C stretch

The fragment consists of two N-methylpyrrole rings connected by a peptide linkage and is shown in Figure 3c. The inertial effects of the side chains (and the additional pyrrole in distamycin) are modelled through effective masses. This structure is chosen as the simplest model which gives information about two interesting vibrational effects. First, the changes in peptide modes resulting from vibrational interactions with the pyrroles can be investigated. Second, the changes in the individual pyrrole modes when loosely coupled by a peptide linkage can be seen. Force fields for N-methylpyrrole and the peptide group were combined to describe this fragment. (See App.4). Ring force constants were adjusted slightly to compensate for possible small conjugation effects. The calculated frequencies for this fragment are shown in Table 4. together with a description of the normal modes. In this calculation both effective masses are set equal to 12 amu. and the molecular backbone is specified to be planar (see Figure 3). Varying the end masses from 12 to 80 amu. and adjusting the dihedral angles of the fragment had a negligible effect on the frequencies of most normal modes. The largest frequency variations resulted from adjusting the end masses and involved mainly two sets of calculated frequencies. One of these included the frequencies at 1572, 1594, 1622 and 1631 cm^{-1} calculated to involve ring C=C stretches. The largest shift encountered was approximately 40 cm^{-1}. In addition smaller shifts were noted in the frequencies calculated between 1150 and 1250 cm^{-1}. These normal modes involved mainly interplane C-H bending. Smaller variations (20 cm^{-1}) were noted in individual bands calculated at 1010 cm^{-1} (interplane ring stretch and bend) and 1360 cm^{-1} (interplane ring stretch). These frequency

Table 4. Observed and Calculated Frequencies and Assignments for Distamycin

Note: The numbers 1 and 2 in parenthesis refer to the pyrrole rings on the carboxyl and amide sides of the peptide link respectively.

Observed Raman Frequencies for Distamycin	Calculated Frequencies and Modes for Model Fragment	
cm^{-1}	cm^{-1} (*)	Mode
1010	998 (2) 1010 (1)	Interplane ring stretch and bend
1066	1059 (1) 1060 (2)	Methyl rock and pyrrole N-C stretch
1113	1113 (2) 1119 (1)	Methyl rock
1145	1152 (2)	Interplane C-H bend and stretch
1168	1179 (1)	Interplane C-H bend
1209	1192 (1) 1195 (2)	Interplane C-H bend
1230	1224 (2)	Interplane C-H bend and stretch
1278	1278	Amide III.
1354 1368	1356 (1) 1360 (2)	Interplane ring C-C, C=C stretches
1396-1400	1398 (2) 1403 (1)	N-C ring stretch
1412	1408 (1,2) 1409 (1,2)	Methyl symmetric bend
1440	1437 (2) 1438 (1)	Methyl symmetric bend
	1452 (1,2)	Methyl symmetric bend
	1452 (1,2)	Methyl symmetric bend

Table 4. (Continued)

Observed Raman Frequencies for Distamycin	Calculated Frequencies and Modes for Model Fragment	
cm^{-1}	cm^{-1} (*)	Mode
	1452 (1,2)	Methyl antisymmetric bend
	1452 (1,2)	Methyl antisymmetric bend
1485	1481 (1)	
	1493 (2)	Ring N-C stretch
	1512 (1)	Ring C=C stretch
	1556 (2)	Ring C=C torsion
	1572 (2)	Ring C=C stretch
1583	1594	Amide and Ring C=C stretch
1620-1640	1622	
	1631	Ring C=C stretch
	1680	Amide I

shifts were significant for lines whose assignments were already tentative and not central to the major conclusions of this work.

Raman Spectra of Netropsin and Distamycin A

Solution spectra of both netropsin and distamycin A are shown in Figure 11. Bands in the distamycin spectrum are stronger (relative to the water band at 1645 cm^{-1}) due to the higher concentration of this drug. The distamycin spectrum also has a higher signal-to-noise ratio for this reason. There is a general correspondence between the relative intensities and frequencies of many bands. This implies that these Raman bands arise from similar portions of the drugs. Several differences in frequency and relative intensity are noted in the 1175 to 1300 cm^{-1} region. One weak band occurs near 985 cm^{-1} in the spectrum of netropsin, but is absent in the spectrum of distamycin. Additional very weak bands were observed in the low frequency regions of spectra from concentrated distamycin spectra (Figure 12). Higher sample concentrations than were possible with netropsin were needed in order to be able to observe these bands.

The frequencies of the distamycin A spectrum are also given in Table 4. The correspondence between a number of observed and calculated frequencies is very good and leads to confident assignments for many observed lines. The strong band near 1440 cm^{-1} is assigned to a pure methyl antisymmetric bending mode. Calculated frequencies occur at 1437.0 and 1438.1 cm^{-1} for the vibrations of the two methyl groups. The adjacent band at 1412 cm^{-1} is assigned to a symmetric methyl bend. The two calculated frequencies for this mode are near 1408.5 cm^{-1} and are split by only 0.5 cm^{-1}. Calculations show that for each of these two

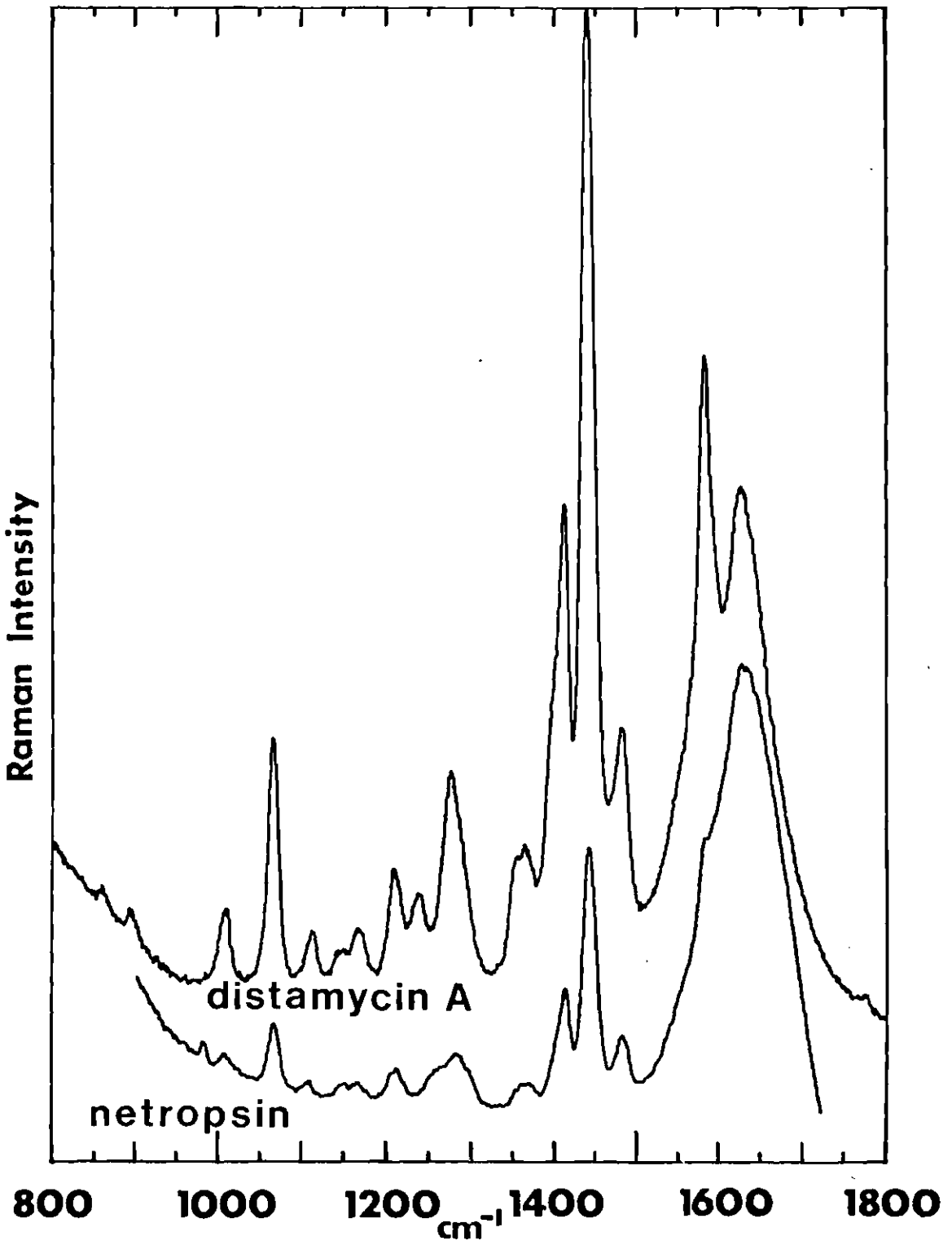

Figure 11. Distamycin A and Netropsin Spectra (950 cm^{-1}).

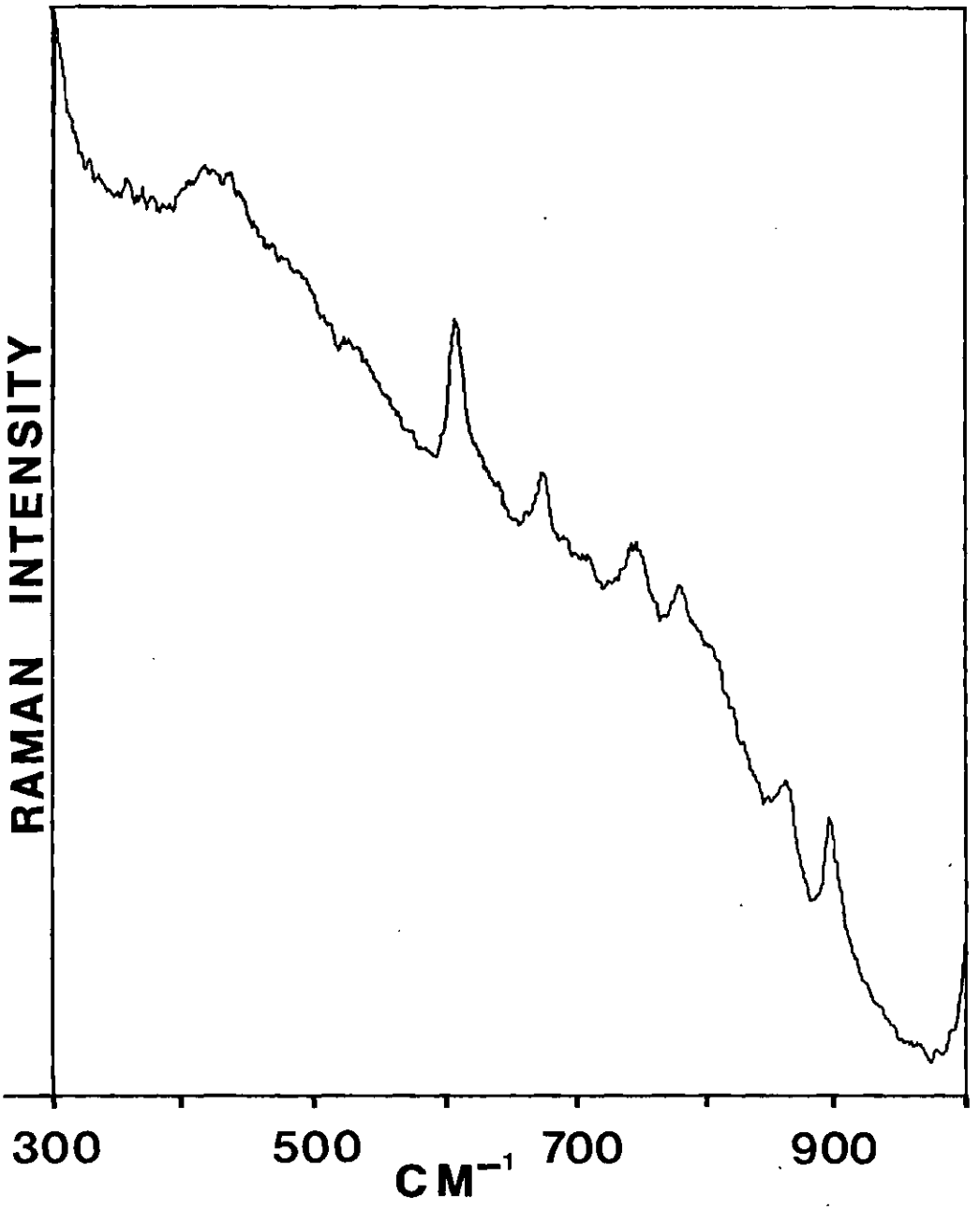

Figure 12. Distamycin A Low and Frequency Spectrum.

modes the potential energy is split in an approximate 30%/70% ratio between the two methyl groups. Two additional lines are assigned to pyrrole methyl rocking motions. These lines are calculated at 1060 and near 1116 cm^{-1} and observed at 1066 and 1113 cm^{-1} respectively. The calculated components of the latter frequency are split by 5 cm^{-1} and represent pure methyl rocking motion. The potential energy of the 1060 cm^{-1} mode is distributed between methyl rocking (60%) and various ring deformations (20% N-C stretches, 10% C-H in plane bends, etc.). The band observed at 1278 cm^{-1} is assigned to a mode which predominantly involves motions of the peptide group (amide III). The calculated mode was at the same frequency. Several bands are assigned to pyrrole ring deformations. Those occurring at 1010 cm^{-1} and around 1360 cm^{-1} involve mainly C-C stretching. At 1485 cm^{-1} a band is assigned mainly to ring N-C stretching with significant additional backbone deformations. Two additional modes involving mainly ring N-C stretching are calculated at 1398 and 1403 cm^{-1}. A shoulder of the 1412 cm^{-1} band is observed in this region. Subtraction of the broad water band near 1645 cm^{-1} (HOH bending) from the distamycin-buffer spectrum also indicates the presence of an additional band at 1630 cm^{-1} (see Figure 13). Two pyrrole ring modes (predominantly C=C stretch) are calculated to be at 1622 and 1631 cm^{-1}. These may give rise to the intensity noted in this region of the unbound distamycin spectra. The NCA predicts bands in the region between 1150 and 1225 cm^{-1} due to in-plane bends of hydrogens attached to the pyrrole rings. Four weak bands observed in this region are therefore assigned as C-H in-plane bends. For these four bands, however, the mean discrepancy between calculated and observed frequencies

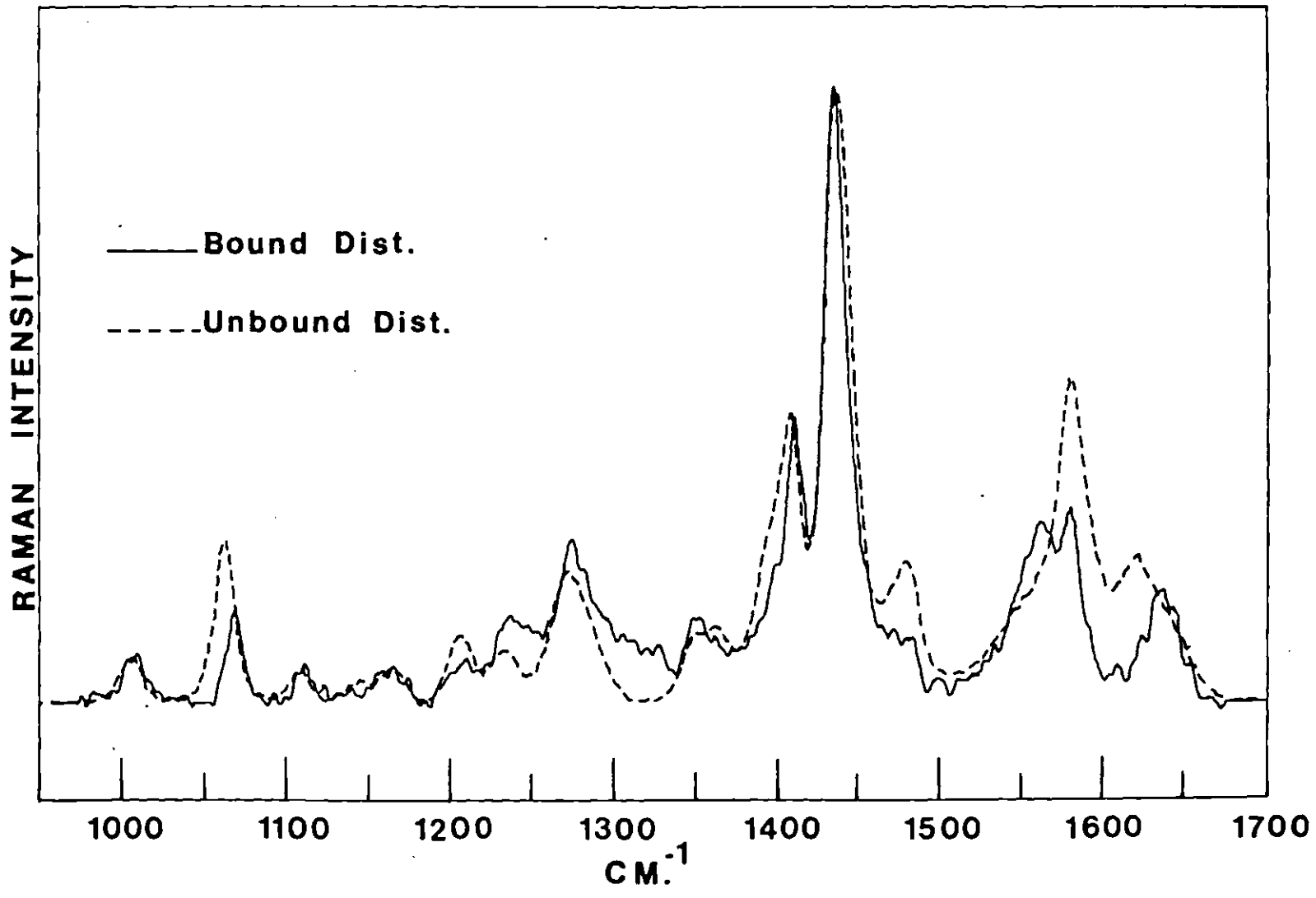

Figure 13. Raman Spectra of Bound and Unbound Distamycin A.

is 13 cm^{-1} compared to 4 cm^{-1} for the previous assignments, and hence must be considered more tentative. A strong band observed at 1583 cm^{-1} lies halfway between calculated frequencies at 1572 and 1594 cm^{-1}. Both calculated modes involve the stretching of ring bonds, while the latter also involves C-N and C=O stretching within the peptide group (32% PED). Although a specific assignment of the 1583 cm^{-1} band cannot be made, it is likely to involve ring stretching.

Drug-DNA Complexes

Figure 13 shows the spectra of free distamycin and distamycin bound to calf thymus DNA. Comparison of the bound and unbound distamycin spectra shows that with the exception of the 1066 cm^{-1} band, all bands assigned to methyl vibrations remain unchanged. To the experimental resolution the intensity and position of the distamycin bands at 1412, 1113, and 1440 cm^{-1} are unaltered upon binding. The PED calculations indicate that these three modes involve purely methyl vibrations. The 1066 cm^{-1} band, which decreases by 60 percent, is assigned to a mode which involves significant ring deformations in addition to methyl rocking. Thus the change in this band may be due to alterations in the vibrations of the pyrrole rings rather than methyl vibrations. This interpretation is supported by the observation that both bands assigned to ring N-C stretching (the shoulder at 1398 cm^{-1} and the band at 1485 cm^{-1}) show large intensity decreases in bound distamycin. In addition the band at 1583 cm^{-1} (which was tentatively assigned to pyrrole ring stretching) splits into two components at 1567 and 1583 cm^{-1}. Unfortunately the presence of a DNA band at 1581 cm^{-1} complicates the evaluation of the relative intensities of these two bands. Figure 13 shows

that if this DNA band remains unchanged upon drug binding then the two bound drug bands have equal intensities. Even if the DNA band did decrease, some change in the drug band is evident. In the unlikely case that the DNA band disappears completely upon drug binding, the 1583 cm^{-1} band would retain most of its intensity. However, the intensity at 1567 cm^{-1} would produce a distinct shoulder on the 1583 cm^{-1} band. Thus some change at 1583 cm^{-1} must occur. The band near 1630 cm^{-1} in the unbound drug (tentatively assigned to pyrrole C=C stretching) shifts upward in frequency about 20 cm^{-1} upon binding.

This shift appears to be real despite considerable noise due to the large water band subtracted from this region. Small changes occur in the bands at 1209, 1240 and 1278 cm^{-1}. The irregular nature and size of the changes and the overlapping of the DNA background makes it difficult to quantify these variations with confidence. The reproducible changes in intensity observed in the 1270 to 1340 cm^{-1} region are consistent with hydrogen bonding between peptide N-H groups and DNA. Chen and Lord[48] observed a correlation between an upward shift of the amide III band and increased hydrogen bond strength for several homopolypeptides. The upward shift we observed is consistent with a change from N-H bonding with water to stronger hydrogen bonds with DNA. The changes of the bands at 1066, 1398, and 1485 cm^{-1} and the lack of change at 1412 cm^{-1} and 1440 cm^{-1} were also observed in netropsin complexes with calf thymus DNA and $(dA\text{-}dT)_n \cdot (dA\text{-}dT)_n$. Because of the reduced drug solubility of netropsin compared to distamycin, the signal to noise ratios were smaller. Thus it was impossible to compare the variation in netropsin's weaker bands with their counterparts in distamycin.

CHAPTER V

CONCLUSIONS

Summary of Binding Results

Several spectral features assigned to specific vibrational modes of netropsin and distamycin are observed to change when these drugs form complexes with DNA. However, other bands appear to be unaffected by the binding process. The behavior of these features taken together suggests a consistent pattern of vibrational changes upon binding.

Raman bands at 1113 (distamycin only), 1412 and 1440 cm^{-1} (assigned to vibrational modes involving solely the methyl groups of pyrrole) are unaffected by binding. Changes noted in the 1066 cm^{-1} band can be attributed to a decrease in the pyrrole ring N-C stretching character of this mode. According to this reasoning, the mixed mode becomes more like a pure methyl rocking mode upon binding. The group frequency of such a pure methyl rocking mode is approximately 50 cm^{-1} higher (than 1066 cm^{-1})[40].

This could explain the observed intensity decrease and frequency increase of the 1066 cm^{-1} band upon binding. Several bands assigned to vibrational modes of the pyrrole rings are changed upon binding. Particularly, bands assigned mainly to stretches of the ring N-C bonds (at 1398 and 1485 cm^{-1}) are observed to decrease in intensity. In distamycin bands at 1583 and 1630 cm^{-1} (tentatively assigned to ring stretches) shift in frequency. These changes indicated in the pyrrole vibrations occur despite the absence of change in modes of the nearby

methyl groups. This makes it unlikely that the changes result from direct interaction of the DNA with the regions of the drug close to the pyrrole nitrogens. For distamycin changes are observed in the amide III band assigned to the peptide groups (1278 cm^{-1}). These groups are attached to the pyrrole rings on the opposite sides from the methyl groups and are known to participate readily in hydrogen bonding[13]. Thus, interactions between the peptide groups and DNA could explain the changes in the ring modes. These variations could occur through such mechanisms as the induction of stress in the rings and changes in π electron distribution along the drug backbone.

These results provide physical evidence for a binding model for netropsin-DNA and distamycin-DNA complexes which includes these features:

1. The environment of the pyrrole methyl groups is unchanged by DNA binding.
2. The pyrrole rings themselves are affected by the binding interactions.
3. The N-H vibrations of the peptide groups are affected by binding.

These features were used together with previously established characteristics of the binding of these drugs to DNA to investigate possible binding geometries. A CPK model of B form DNA was constructed and conformational angles were "fine tuned" to give the helical pitch, separation of adjacent base pairs, and span across the helix found by X-ray crystallography[49]. The estimated residual error in these

distances was 10 percent of the distance involved. Similar models of the two drugs were constructed. Free rotation was allowed in CPK drug models, except within rings and peptide linkages which were made separately planar.

Geometric Features of the Binding Model

For drug binding in the minor groove of DNA (and consistent with the features above) model building studies show that the methyl groups project outward from the helical axis. This orientation has been suggested as a feature of previous binding models[50]. Direct physical confirmation of it has been lacking for distamycin-DNA and netropsin-DNA complexes. Evidence in agreement with this finding is the observation that substitution of a propyl group in the 1-position of the pyrrole rings of distamycin does not significantly alter its binding[50]. Thus pyrrole ring N1 positions of these drugs are logical sites for chemical modifications aimed at creating cell uptake selectivity while maintaining DNA binding activity.

We have found by geometrical calculations and model building that the central portions of both drugs can form several hydrogen bonding contacts with DNA. This arrangement is consistent with the methyl orientation described above. In this model peptide hydrogens make good contact with hydrogen bond acceptor sites in the minor groove (O2 of thymine and the N3 of adenine) of the DNA. This matching is especially close for the three peptide hydrogens (two for netropsin) toward the propionamidino end of the drugs. (The replacement of adenine and thymine bases by guanine and cytosine diminishes the degree

of stereochemical fit only slightly although the electronic reactivity may change greatly.) This model suggests that the drug binds along a single strand of DNA. It further requires that the propionamidino end of the drugs point toward the 3' end of this strand. Although the spacing of hydrogen bonding donor and acceptor sites are very similar with the reversed orientation, serious steric contacts with the wall of the minor groove preclude binding.

The binding arrangement described above requires that both dihedral angles ϕ and ψ be small ($< 30^{\circ}$). A model which suggests a similar arrangement has been proposed by Zasedatelev, et al[50]. However, they report dihedral angles of $\phi = 140^{\circ}$ and $\psi = 60^{\circ}$ (using the same angle conventions as in this study). This requires that the methyl groups of successive pyrroles point away from the drug backbone in almost opposite directions.

This seems to be inconsistent with our results and their own description of their binding model. The reason for this discrepancy is unclear and may be trivial.

The present study did not confirm an earlier suggestion[50] of contacts between the positively charged propionamidino side chain and the DNA phosphate groups. This study suggests rather that this end may contact an oxygen of either the next ribose or base.

Other models were also investigated in which the drug bound across the DNA strands. These models had the drawbacks of providing hydrogen bonding contacts mostly with ribose oxygens rather than with bases. This seems to be inconsistent with the strong A-T binding specificity.

APPENDICES

APPENDIX A

The radiated power from a particle (with charge q and acceleration A) is given by classical electromagnetic theory as:

$$p = \frac{2q^2 a^2}{3c^3} \tag{A-1}$$

In this case the acceleration occurs in response to an external electromagnetic field due to light. The displacement of the particle may then be taken as:

$$X = X_o \sin (2\pi\nu t) \tag{A-2}$$

(where is the frequency of oscillation.) The square of the resulting acceleration is:

$$A^2 = 16\ \pi^4\ \nu^4\ X_o^2\ \sin^2\ (2\pi\nu t) \tag{A-3}$$

The emitted power is then:

$$p = \frac{2q^2\ 16\ \pi^4\ \nu^4\ X_o^2\ \sin^2\ (2\pi\nu t)}{3c^3} \tag{A-4}$$

When this expression is time averaged the $\sin^2\ (2\pi\nu t)$ factor becomes $\frac{1}{2}$ and the average power emitted is:

$$\overline{p} = \frac{16\ \pi^4\ \nu^4\ \ q^2\ X_o^2}{3c^3} \tag{A-5}$$

The electric dipole moment μ of such a system is the product of the charge of the particle times its displacement and thus is also oscillatory:

$$\mu = qX = qX_o \sin (2\pi\nu t)$$

$$\mu = \mu_o \sin (2\pi\nu t) \tag{A-6}$$

where $\mu_o = qX_o$ is the maximum magnitude of the electric dipole moment μ. Finally, the average emitted power may be written in terms of the dipole moment as:

$$\overline{P} = \frac{2\left[\frac{\partial^2 \mu}{\partial t^2}\right]^2}{3C^3} \tag{A-7}$$

or

$$\overline{P} = \frac{16\,\pi^4\,\nu^4}{3C^3}\ \mu_o^2 \tag{A-8}$$

The dipole moment for a group of charged particles may be formed by vector addition of the contributions from individual particles. In dealing with bulk samples an intensive quantity, the polarization $\vec{P}$, is used. This is defined as the electric dipole moment per unit volume:

$$\vec{P} = \frac{\vec{\mu}}{V} = \frac{\vec{\mu}_o}{V} \sin (2\pi\nu t) \tag{A-9}$$

Taking the second time derivative of P yields:

$$\frac{\partial^2 P}{\partial t^2} = - 4\pi^2\,\nu^2\,\frac{\mu_o}{V} \sin (2\pi\nu t) \tag{A-10}$$

Upon squaring and time averaging Eq.(A-10), the result is similar to the right side of Eq. (A-8):

$$\left(\frac{\partial^2 P}{\partial t^2}\right)^2 = 16\,\pi^4\,\nu^4\,\frac{\mu_o^2}{V^2}\,\left(\frac{1}{2}\right) \tag{A-11}$$

Thus Eq. (A-8) may be written as:

$$\overline{P} = \frac{2V^2\left(\frac{\partial^2 P}{\partial t^2}\right)^2}{3C^3} \tag{A-12}$$

APPENDIX B

In order to describe the time dependence of $\vec{P}(\vec{E})$ (which results mainly from the application of an external electric field) the small effects of molecular vibrations must be considered. In normal vibrations of a molecule, all atoms move in phase with each other (i.e. pass through positions of maximum displacement simultaneously). Thus for each normal mode of vibration (with frequency ν) a single parameter X_ν may be used to indicate the vibrational state of all atoms as a function of time. This parameter will be used in the analysis of the third term in the Taylor series expansion in Equation (A-13) for $\vec{P}(\vec{E})$. Recall that the external electric field is required to be very small (compared to the ambient intermolecular electric field) in order to nelgect further terms. The third term may be written:

$$\frac{1}{2} \sum_{j=1}^{3} \sum_{k=1}^{3} \frac{\partial \alpha_j}{\partial X_\nu} \frac{\partial X_\nu}{\partial E_k} E_k E_j = \frac{1}{2} \left(\sum_{k=1}^{3} \frac{\partial \alpha_\nu}{\partial E_k} E_k \right) \sum_{j=1}^{3} \frac{\partial \alpha_j}{\partial X_\nu} E_j \qquad \text{(B-1)}$$

using the chain rule.

The total differential of a function $W(X_1, X_2, X_3)$ is defined as:

$$dW = \frac{\partial W}{\partial X_1} dX_1 = \frac{\partial W}{\partial X_2} dX_2 + \frac{\partial W}{\partial X_3} = \sum_{k=1}^{3} \frac{\partial W}{\partial X_k} dX_k \qquad \text{(B-2)}$$

If however we associate dX_k with finite increments ΔX_k in the values of X_k, then there results an approximation:

$$\Delta W = \sum_{k=1}^{3} \frac{\partial W}{\partial X_k} \Delta X_k \qquad \text{(B-3)}$$

This approximation to the increment of W is most valid when the increments ΔX_k are very small. The expression in parenthesis in Equation (A-12) may then be recognized as the increment in the parameter X_ν. Upon defining the rate of change of polarizability with vibrational coordinate as $\vec{\beta}_j^{\,\nu}$, the third term may be written:

$$\frac{1}{2} X_\nu \sum_{j=1}^{3} \vec{\beta}_{oj}^{\,\nu} E_j$$

(The o subscript indicates that these derivatives are evaluated at $X_\nu = 0$.) As with the second term this predicts a tensor relationship between $\vec{E}$ and $\vec{p}$, with the elements of the tensor now given by:

$$\beta_{ij}^{\,\nu} = \frac{\partial \alpha_{ij}}{\partial X_\nu} \qquad \text{(B-4)}$$

Summarizing, we have:

$$\vec{p}(\vec{E}) = \vec{p}(\vec{E}=o) + \sum_{i=1}^{3} \vec{\alpha}_i E_i + \frac{1}{2} X_\nu \sum_{j=1}^{3} \vec{\beta}_j E_j \qquad \text{(B-5)}$$

Let the time dependence of the electric field of the light be given by:

$$E_k = E_{ko} \cos 2\pi\nu_\ell t \qquad \text{(B-6)}$$

For small vibrations the atoms will oscillate harmonically and X_ν may be given as:

$$X_\nu = X_{\nu o} \cos 2\pi\nu t \qquad \text{(B-7)}$$

The polarization then has the form:

$$\vec{p}(\vec{E}) = \vec{p}(\vec{E} = o) + \left(\sum_{i=1}^{3} \vec{\alpha}_{oi} E_{io} \right) \cos 2\pi \nu_{\ell} t$$

$$+ \left(\frac{1}{2} X_{\nu o} \sum_{j=1}^{3} \vec{\beta}_{oj} E_{jo}\right) \cos 2\pi \nu_{\ell} t \cos 2\pi \nu t \qquad \text{(B-8)}$$

By using the trigonometric identiy

$$\cos X \cos Y = \frac{1}{2} (\cos (X + Y) + \cos (X - Y)) \qquad \text{(B-9)}$$

the last term may be expressed differently:

$$\vec{p}(\vec{E}) = \vec{p}(\vec{E}=o) + \left(\sum_{i=1}^{3} \vec{\alpha}_{oi} E_{io} \right) \cos 2\pi \nu_{\ell} t$$

$$+ \left(\frac{1}{4} X_{o} \sum_{j=1}^{3} \vec{\beta}_{oj} E_{jo}\right) (\cos 2\pi(\nu_{\ell}+\nu)t + \cos 2\pi(\nu_{\ell}-\nu)t \qquad \text{(B-10)}$$

This equation may be expressed simply in matrix notation:

$$\vec{p}(\vec{E}) = \vec{p}(\vec{E}=o) + \boldsymbol{\alpha}_{o} \vec{E}_{o} \cos 2\pi \nu_{\ell} t \qquad \text{(B-11)}$$

$$+ \frac{1}{4} X_{\nu o} \boldsymbol{\beta}_{o} \vec{E}_{o} (\cos 2\pi(\nu_{\ell}+\nu)t + \cos 2\pi(\nu_{\ell}-\nu)t) \qquad \text{(B-11)}$$

And finally by defining

$$\vec{p}_{o} = \vec{p}(\vec{E}=o), \ \vec{A}_{o} = \boldsymbol{\alpha}_{o} \vec{E}_{o}, \ \vec{B}_{o} = \frac{X_{\nu o}}{4} \boldsymbol{\beta}_{o} \vec{E}_{o} \qquad \text{(B-12)}$$

it may be written as:

$$\vec{p}(\vec{E}) = \vec{p}_{o} + \vec{A}_{o} \cos 2\Pi\nu_{\ell} t + \vec{B}_{o} (\cos 2\pi(\nu_{\ell}+\nu)t + \cos 2\pi(\nu_{\ell}-\nu)t) \qquad \text{(B-13)}$$

APPENDIX C

We wish to show that for a system having distinct eigenvalues:

$$\mathbf{A'MA=1} \tag{III-12}$$

The element $(\mathbf{A'MA})_{\ell k}$ may be written explicitly as:

$$(A'MA)_{\ell k} = \sum_i A'_{\ell i} \sum_{i\ell} M_{i\ell}\, A_{\ell k} \tag{C-1}$$

$$= \sum_i A_{i\ell} \sum_{\ell} m_i \delta_{i\ell}\, A_{\ell k}$$

$$= \sum_i A_{i\ell}\, A_{ik}\, m_i$$

This in order to establish the desired result we must show that:

$$\sum_i A_{i\ell}\, A'_{ik}\, m_i = \delta_{\ell k} \tag{C-2}$$

Consider two of the secular equations for eigenvalues λ_m and λ_n.

$$\sum_i V_{ji}\, A_{im} = A_{jm}\, m_j\, \lambda_m$$

$$\sum_i V_{ij}\, A_{jn} = A_{in}\, m_i\, \lambda_n \tag{III-8}$$

The left sides of the equations can be made identical by multiplying each equation by the proper factor and summing over the correct index. (Equation a is multiplied by A_{jn} and summed over j, while equation b is multiplied by A_{im} and summed over i.). The symmetry of $\mathbf{V}$ is

$$\sum_{i,j} V_{ij} A_{i\ell} A_{jk} = \lambda_k \sum_i A_{i\ell} A_{ik} m_i$$

$$= \lambda_\ell \sum_j A_{j\ell} A_{jk} m_j \qquad \text{(C-3)}$$

The summations on the right hand sides are identical apart from the dummy index. This gives:

$$o = (\lambda_k - \lambda_\ell) \sum_i A_{i\ell} A_{ik} M_i \qquad \text{(C-4)}$$

if λ_k and λ_ℓ are distinct eigenvalues the sum must be zero:

$$\sum_i A_{i\ell} A_{ik} m_i = 0 \qquad \text{(C-5)}$$

Neither this result nor equation (III-8) fully defines $\mathbf{A}$. The final specification of $\mathbf{A}$ can be made by defining:

$$\sum_i A_{i\ell} A_{ik} m_i = 1 \qquad \text{(C-6)}$$

when $k = \ell$.

Equations (C-5) and (C-6) are then equivalent to the desired result (Eq. (C-2)).

APPENDIX D

The force field used for the normal coordinate analysis of the model fragment was quite extensive and is best described by consulting References 44 and 45. Changes were made only in some of the on-diagonal force constants related to the pyrrole rings. These changes are given below.

	Scott[44]		Values Used in this Study	
Coord. no.	Description	Force const.	Ring 1	Ring 2
2	C-H (beta) str.	5.310	same	5.500
6	C-C stretch	5.999	6.470	6.600
7	C=C stretch	8.366	8.200	8.200
8	C-N stretch	7.695	7.930	8.000
15	H-C*-H bend	0.536	0.515	0.515
50	N-C*-H bend	0.797	0.789	0.789

BIBLIOGRAPHY

1. C. Zimmer, in "Prog. Nuc. Acid Res. & Mol. Biol.," W. E. Cohn, Ed., (Acad. Press, Inc., N.Y.) 285 (1975).

2. F. M. Schabel, W. R. Laster, R. W. Brockman and H. E. Skipper, PSEMB, 83, 1 (1953).

3. G. H. Werner and R. Maral, Actual. Pharmaceut. Fr., 21, 133 (1963).

4. H. Thrum, I. Haupt, G. Bradler, C. Zimmer and K. E. Reinert, in "Antimicrobial and Antineoplastic Chemotherapy," (Czech. Med. Press, Prague) Vol. 1/2, 819 (1972).

5. M. Verini and M. Ghione, Chemotherapia, 9, 144 (1964).

6. G. H. Werner, P. Ganter and Y. de Ratuld, Chemotherapia, 9, 65 (1964).

7. J. Fournel, P. Ganter, F. Koenig, Y. de Ratuld and G. H. Werner, in "Antimicrobial Agents and Chemotherapy," G. L. Hobby, Ed., (American Society for Microbiology, Detroit), 599 (1965).

8. A. M. Casazza, A. Fioretti, M. Ghione, M. Soldati and M. A. Verini, in "Antimicrobal Agents and Chemotherapy," G. L. Hobby, Ed., American Society for Microbiology, Detroit), 593 (1965).

9. Y. de Ratuld and G. M. Werner, in "Progress in Antimicrobial and Anticancer Chemotherpy, " (Univ. Tokyo Press, Toko), Vol. 2, 14, (1970).

10. A. Fioretti, Atti. Congr. Soc. Ital. Microbiol., 14 1, (1967).

11. P. Chandra, A. Gotz, A. Wacker, M. A. Verini, A. M. Casazza, A. Fioretti, F. Arcamone and M. Ghione, FEBS Lett., 16, 249 (1971).

12. F. E. Hahn, in "Antiobiotics," J. W. Corcoran and F. E. Hahn, Eds., (Springer-Verlag, Berlin and New York), Vol. 3, 79 (1975).

13. A. Lehninger, "Biochemistry," (Worth Publishers, Inc., N.Y.), 1970.

14. S. Lin and A. D. Riggs, Cell, 4, 107, (1975).

15. P. H. Von Hippel and J. D. McGhee, Ann. Rev. Biochem., 41, 231 (1972).

16. C. W. Waller, C. F. Wolf, W. J. Stein and B. L. Hutchings, JACS, 79, 1265 (1957).

17. S. Nakamura, H. Yonehara and H. Umezawa, J. Antibiot., 17 220 (1964).

18. F. Arcamone, S. Penco, V. Nicolella, P. Orezzi and A. Pirelli, Nature (London) 203, 1064 (1964).

19. F. Arcamone, G. P. Orezzi, W. Barbieri, V. Nicolella and S. Penco, Gazz. Chimica Ital., 97, 1097 (1967).

20. S. Penco, S. Redaelli, F. Arcamone, Gazz. Chimica Ital., 97, 1110 (1967).

21. C. Zimmer, K. E. Reinert, G. Luck, U. Wahnert, G. Lober, and H. Thrum, J. Mol. Biol., 58, 329 (1971).

22. R. M. Wartell, J. E. Larson and R. D. Wells, J. Biol. Chem., 249, 6719 (1974).

23. A. K. Krey, R. G. Allison and F. E. Hahn, FEBS Lett., 29, 58 (1973).

24. A. S. Zasedatelev, G. V. Gursky, C. Zimmer, and H. Thrum, Mol. Biol. Rep., 1, 337 (1974).

25. D. J. Patel and L. L. Canuel, Proc. Nat. Acad. Sci. USA, 74, 5207 (1977).

26. G. Luck, H. Triebel, M. J. Waring and C. Zimmer, Nuc. Acid Res., 1, 503 (1974).

27. K. E. Reinert, J. Mol. Biol., 72, 593 (1972).

28. A. M. Kolchinskii, A. D. Mirzabekov, A. S. Zasedatelev, G. V. Gursky, S. L. Grokhovsky, A. L. Zhuse and B. P. Gottich, Molekul. Biol., 9, 19 (1975).

29. A. Smekal, Naturwiss., 11, 873 (1923).

30. C. V. Raman, Nature, 121, 619 (1928).

31. N. T. Yu, CRC Crit. Rev. Biochem., 4, 229 (1977).

32. J. L. Koenig, J. Polymer Science - Part D, 6, 59 (1972).

33. J. D. Jackson, "Classical Electrodynamics," (John Wiley and Sons, Inc., New York), 1962.

34. H. F. Hameka, "Advanced Quantum Chemistry," (Addison-Wesley Publishing Company, Inc., Reading, Massachusetts), 1965.

35. W. Heitler, "The Quantum Theory of Radiation," (Oxford Claredon Press, Oxford) 3 edn., 1954.

36. S. Califano, "Vibrational States," (John Wiley and Sons, Ltd., London), 1976.

37. A. Laubereau, D. Vonder Linde and W. Kaiser, Phys. Rev. Lett., 28, 1162 (1972).

38. L. D. Landau and E. M. Lifshitz, "Statistical Physics," (Pergamon Press Ltd., London), 1958.

39. F. R. Dollish, W. G. Fateley and F. F. Bentley, "Characteristic Raman Frequencies of Organic Compounds," (J. Wiley and Sons, Inc., New York), 1974.

40. N. B. Colthup, L. H. Daly and S. E. Wiberley, "Introduction to Infrared and Raman Spectroscopy," (Academic Press, New York), 2 edn., 1975.

41. H. Goldstein, "Classical Mechanics," (Addison-Wesley Publishing Company, Inc., Reading, Mass.), 1950.

42. E. B. Wilson, Jr., J. C. Decius, and P. C. Cross, "Molecular Vibrations," (McGraw-Hill Book Company, New York), 1955.

43. W. D. Gwinn, J. Chem. Phys. 55, 477 (1971).

44. D. W. Scott, J. Mol. Spect. 37, 77 (1971).

45. J. Jakes and S. Krimm Spect. Acta, 27A, 19 (1971).

46. T. Miyazawa and K. Fukushima, J. Mol. Spect., 15, 308 (1965).

47. P. Adamek, K. Volka, Z. Ksandr and I. Stibor, J. Mol. Spect., 47, 252 (1973).

48. M. C. Chen and R. C. Lord, J. Am. Chem. Soc., 96, 4750 (1974).

49. S. Arnott and D. W. L. Hukins, J. Mol. Biol., 81, 93 (1973).

50. A. S. Zasedatelev, A. L. Zhuke, K. Tsimmer, S. L. Grokhovsky, V. G. Tumanyan, G. V. Gursky, and B. P. Gottich, Dokl. Akad. Nauk (USSR), 234, 1006 (1976).

VITA

James Carey Martin was born on March 1, 1947 in Ozark, Alabama, the son of Percy and Lucile Martin. Upon graduation from Carroll High School in 1965, he attended Case Institute of Technology in Cleveland, Ohio and Florida State University, from which he received a Bachelor of Science in Physics in 1969.

In September of 1968 he married Kathleen Andrews.

During his graduate study at Georgia Institute of Technology he has held teaching and research assistantships in addition to teaching at Yeshiva High School of Atlanta and The Lovett School.

His research was done under the direction of Dr. D. C. O'Shea.